DermaCon-IN: A Multi-concept Annotated Dermatological Image Dataset of Indian Skin Disorders for Clinical AI Research

Shanawaj S Madarkar[*†‡]   **Mahajabeen Madarkar**[*§]   **Madhumitha V**[*†]

Teli Prakash[¶]   Konda Reddy Mopuri[†]   Vinaykumar MV[‖]   KVL Sathwika[**]

Adarsh Kasturi[**]   Gandla Dilip Raj[**]   PVN Supranitha[**]   Harsh Udai[†]

Abstract

Artificial intelligence is poised to augment dermatological care by enabling scalable image-based diagnostics. Yet, the development of robust and equitable models remains hindered by datasets that fail to capture the clinical and demographic complexity of real-world practice. This complexity stems from region-specific disease distributions, wide variation in skin tones, and the underrepresentation of outpatient scenarios from non-Western populations. We introduce DermaCon-IN, a prospectively curated dermatology dataset comprising over 5,450 clinical images from approximately 3,000 patients across outpatient clinics in South India. Each image is annotated by board-certified dermatologists with over 240 distinct diagnoses, structured under a hierarchical, etiology-based taxonomy adapted from Rook's classification. The dataset captures a wide spectrum of dermatologic conditions and tonal variation commonly seen in Indian outpatient care. We benchmark a range of architectures—including convolutional models (ResNet, DenseNet, EfficientNet), transformer-based models (ViT, MaxViT, Swin), and Concept Bottleneck Models to establish baseline performance and explore how anatomical and concept-level cues may be integrated. These results are intended to guide future efforts toward interpretable and clinically realistic models. DermaCon-IN provides a scalable and representative foundation for advancing dermatology AI in real-world settings.

1 Introduction

Skin diseases pose a significant global health challenge, affecting billions of individuals and ranking among the leading causes of disease burden. The Global Burden of Disease 2019 [36] study identified dermatological conditions as the *fourth* leading cause of nonfatal morbidity worldwide. Common ailments such as fungal infections, acne, scabies, and eczema impact millions globally [20], underscoring the urgent need for improved diagnostic tools and equitable access to care.

Artificial intelligence (AI) has emerged as a promising solution for enhancing dermatological diagnosis and triage, particularly in resource-constrained regions with limited access to dermatologists. However, a critical bottleneck remains: the lack of representative training data that adequately

---

[*]Equal contribution

[†]Department of Artificial Intelligence, Indian Institute of Technology Hyderabad, India

[‡]Indian Navy

[§]Department of Dermatology, S R Patil Medical College, India

[¶]Department of Dermatology, S Nijalingappa Medical College, India

[‖]Department of Dermatology, Sri Chamundeshwari Medical College, Hospital & Research, India

[**]Interns at Indian Institute of Technology Hyderabad, India

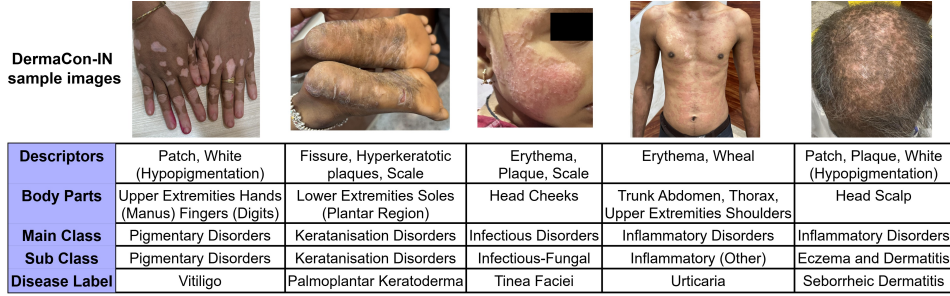| DermaCon-IN sample images					
Descriptors	Patch, White (Hypopigmentation)	Fissure, Hyperkeratotic plaques, Scale	Erythema, Plaque, Scale	Erythema, Wheal	Patch, Plaque, White (Hypopigmentation)
Body Parts	Upper Extremities Hands (Manus) Fingers (Digits)	Lower Extremities Soles (Plantar Region)	Head Cheeks	Trunk Abdomen, Thorax, Upper Extremities Shoulders	Head Scalp
Main Class	Pigmentary Disorders	Keratanisation Disorders	Infectious Disorders	Inflammatory Disorders	Inflammatory Disorders
Sub Class	Pigmentary Disorders	Keratanisation Disorders	Infectious-Fungal	Inflammatory (Other)	Eczema and Dermatitis
Disease Label	Vitiligo	Palmoplantar Keratoderma	Tinea Faciei	Urticaria	Seborrheic Dermatitis

Figure 1: Sample images from DermaCon-IN dataset with skin lesion descriptors, body parts, main class, sub class, and disease labels.

captures diversity in disease presentations and skin tones based on regional relevance [4]. Most AI models for dermatology to date have been developed and benchmarked using datasets predominantly sourced from North American, European, or Australasian populations [1, 25]. This geographic skew has introduced performance biases, especially for underrepresented groups such as individuals, patients presenting with diseases more prevalent outside Western contexts, and with darker skin tones.

Recent work reveals the consequences of biased dermatology datasets [1, 27]. Public benchmarks focus on pigmented lesions and melanoma, mirroring Western priorities, while overlooking common conditions in tropical regions, like fungal infections, scabies, pigmentary, and nutritional disorders [34, 36, 20, 11, 19]. A "one-size-for-all" approach fails across populations, demanding region-specific resources. Under-representation of darker skin tones compounds this gap: [4] reports 30-40% accuracy drop on darker skin in DDI, while trained on Fitzpatrick17k's dataset (dominant lighter tones in the dataset). These biases lead to models that underperform on underrepresented phenotypes.

To address these limitations, we introduce a new dermatology image dataset curated from Indian outpatient clinics. To the best of our knowledge, it is the first densely annotated dataset centered around Indian skin phototype and is designed to improve diversity in both disease coverage and skin tone representation for dermatological AI research. It complements existing datasets by capturing the phenotypic and pathological landscape of a population historically underserved in global medical AI efforts. In addition, the dataset also aims to support explainable modelling by reflecting how dermatologists diagnose, through the combined use of anatomical location and visual descriptors. The Key contributions of this work are as follows:

- **South Asian Clinical and Phenotypic Representation.** DermaCon-IN developed in South Asia reflects regional disease patterns, such as the high prevalence of infectious etiologies (fungal, viral, parasitic) observed in tropical outpatient settings [39, 12, 32, 2, 18]. This contrasts with existing datasets dominated by inflammatory or neoplastic disorders common in Western contexts [42, 15]. The dataset also includes Fitzpatrick skin types IV–VI, which are typically underrepresented in existing resources [10], offering a path to reduce fairness gaps in clinically deployable AI models.

- **Multi-Concept Clinical Annotations.** Each image is annotated with two independent sets of clinically meaningful metadata: precise anatomical locations and lesion-level descriptors that capture surface and morphological features of skin lesions (seen in Figure 1). To the best of our knowledge, this is the first publicly available dataset to offer both annotation types at this scale and granularity, supporting structured supervision and interpretable modeling.

- **Clinically Aligned Hierarchical Labeling.** Disease labels are organized in a three-tier hierarchy: main diagnostic class, etiology-based subclass, and specific disease label. This structure is derived from Rook's *Textbook of Dermatology* (the clinical gold standard) [9] and adapted to Indian dermatology practice. It mirrors diagnostic workflows in real-world settings, enabling both coarse- and fine-grained modeling.

- **Benchmarking for Classification and Interpretability.** We provide baseline results for disease classification and for Concept Bottleneck Models (CBMs) [22] that leverage the concept annotations. These benchmarks demonstrate the dataset's relevance for both predictive accuracy and to evaluate whether models are learning medically meaningful concepts in alignment with expert reasoning.

2   Related Work

Table 1: Comparative Survey of existing Dermatology Datasets available for AI research [Columns: **A**: Neoplasm & Tumors Centric, **B**: Broad Skin Disease Spectrum, **C**: Dermoscopic Single Lesion Focus, **D**: Real-time Multi-lesion Multi-Focus, **E**: Body Part, **F**: Lesion Descriptor]

Dataset	Disease Distribut.		Acquisit. Type		Dense Annotat.		Source of Images		Skin Tone	Classes	
	A	B	C	D	E	F	Web Scraped (Atlas)	Geographic Location	Present	#Images	Hierarchical #level[#count]
ISIC Archive [17]	✓	✗	✓	✗	✓	✗	✗	Europe	✗	∼485,000	1[9]
HAM10000 [37]	✓	✗	✓	✗	✓	✗	✗	Austria,Australia	✗	10,015	1 [7]
DERM12345 [43]	✓	✗	✓	✗	✗	✗	✗	Türkiye	✗	12,345	3 [5,15,38]
BCN20000 [14]	✓	✗	✓	✗	✓	✗	✗	Spain	✗	18,946	1 [8]
PH2 [26]	✓	✗	✓	✗	✗	✓	✗	Portugal	✗	200	1 [3]
PAD-UFES-20 [28]	✓	✗	✗	✓	✓	✗	✗	Brazil	✗	1,612	1 [6]
DDI [4]	✓	✗	✗	✗	✓	✗	✗	USA	✓	656	1[78]
Derm7pt [21]	✓	✗	✓	✗	✗	✓	✓	Italy	✗	1,011	2 [5, 20]
Fitzpatrick17k [10]	✗	✓	✗	✓	✗	✗	✓	–	✓	16,577	3 [3,9,114]
SD-198 [33]	✗	✓	✗	✓	✗	✓	✓	–	✗	6,584	1[198]
SkinCon [5]	✗	✓	✗	✓	✗	✓	✓	–	✓	3,886	✗
PASSION [8]	✗	✓	✗	✓	✓	✗	✗	Africa	✓	4,901	1[4]
SCIN [40]	✗	✓	✗	✓	✓	✗	crowd-sourced	USA	✓	10,000+	1 [419]
DermaCon-IN	✗	✓	✗	✓	✓	✓	✗	South India	✓	5,450	3 [8,19,254]

Neoplasm-Centric Benchmarks: Early dermatology AI models were trained on datasets focused on neoplasms and tumours, such as the ISIC [17], HAM10000 [37], DERM12345 [43], etc, as discussed in Table 1. These primarily contain dermoscopic images and omit common diseases like infectious and inflammatory disorders. Dermoscopic imaging focusing on a single lesion further abstracts clinical variability in lighting, context, and lesion complexity, limiting real-time applicability.

Atlas-Sourced Clinical Datasets: SD-198 [33] and Fitzpatrick17k [10] introduced clinical (non-dermoscopic) photographs to broaden the coverage of disease spectrum. However, both are derived from educational atlases (like DermNet), not clinical repositories, yielding limited annotations. Moreover, the Fitzpatrick17k [10] dataset excludes several prominent diseases, including Fungal and Viral infections, and has skewed tonal variation of over 75% belonging to Types I–III.

Fairness-Focused Collections: Datasets like DDI [4] and PASSION [8] emphasise tonal representation but trade off diagnostic breadth. DDI includes fewer than 80 disease labels, of which neoplastic or pigmentary offer a larger contribution. PASSION [29] has pediatric participants' images across only four conditions (eczema, fungal infections, scabies, impetigo), selected for regional prevalence. SCIN [40]dataset, on the other hand, introduces crowd-sourced images, expanding coverage to common non-neoplastic conditions but mirrors U.S. disease patterns [23], thus under-representing both high-burden infectious, pigmentary, etc, disorders seen in global contexts and darker skin tones.

Our Dataset in Context: In South Asia, outpatient dermatology is dominated by inflammatory, infectious, pigmentary, and appendageal diseases [39], yet remains underrepresented in existing datasets. We address this gap with a dataset of 5,450 high-resolution clinical images collected prospectively from ∼3,000 Indian patients. It covers the disease

Figure 2: FST and MST distribution of skin tones of subjects in DermaCon-IN dataset

spectrum aligned with Indian and global burden data. Each image retains anatomical context and is annotated by board-certified dermatologists with standardised diagnosis, Fitzpatrick and MST skin tone ratings, distribution of which is shown in Figure 2. Unlike prior work such as Skin-Con [5], which retrofitted a set of lesion descriptors onto existing datasets, we capture both lesion and anatomical concepts at source and leverage the full concept set for statistical validation and model benchmarking.
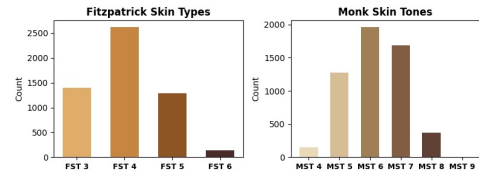
3   Data Collection Methodology

3.1   Clinical Setting and Data Sources

The DermaCon-IN dataset was developed via multi-institutional collaboration involving three tertiary-care hospitals and affiliated regional clinics across North Karnataka, South India. The cohort represents a demographically and geographically diverse outpatient population from Karnataka,

Maharashtra, Goa, and Andhra Pradesh. Data were collected between 2024 and 2025 under institutionally approved ethical protocols.

3.2 Image Acquisition Protocol

Image capture was designed to mirror real-world dermatology workflows, emphasizing both lesion detail and the broader anatomical region. Photographs were taken using high-resolution smartphone devices—108MP Android, 48MP iPhone Pro, and 12–36MP cameras—under ambient clinical lighting. Images include the affected body part with surrounding skin to preserve anatomical context and support spatial modeling. A standardized protocol guided acquisition across sites, allowing relevant variations in angle, distance, and lighting to reflect clinical realism, unlike prior datasets focused on dermoscopic or tightly cropped views.

3.3 Inclusion and Exclusion Criteria

Patients of all ages with clinically confirmed dermatologic conditions were included (with consent), contingent on diagnostic agreement by two board-certified dermatologists or follow-up validation. Only images meeting gradability standards and accompanied by complete metadata, including diagnosis, anatomical region, Fitzpatrick and Monk tone ratings, demographics, and diagnostic confidence, were retained. Exclusion criteria included poor image quality, visual obstructions (e.g., tattoos, accessories), metadata gaps, or ambiguous diagnoses, and patients unwilling to participate.

3.4 Annotation Process

The entire dataset was annotated by four board-certified Dermatologists with clinical experience of 11 years, 3 years, 3 years, and 1 year, respectively. The entire dataset was divided into four smaller subsets for labelling by these doctors based on the availability of the dermatologist. Labels followed a three-level disease taxonomy informed by Rook's Classification [9], which is considered a gold standard in Dermatology (Refer to Supplementary Sec. A). Annotations also included 47 lesion-level descriptors and 49 body part locations, along with patient metadata not linked to patients' privacy. Discrepancies were resolved via consensus or adjudication by a third expert.

3.5 Quality Control and Inter-Rater Agreement

To ensure consistency, 10–15% of each annotator's batch was randomly reviewed by another dermatologist. Inter-rater reliability, measured using Cohen's Kappa, achieved a score of 0.84 (Figure 3), aligning with accepted clinical annotation standards. Skin tone ratings were independently assigned by the set of trained experts, which was verified for consensus by the dermatologist. Anatomical site labels were validated using structured region maps.

Figure 3: Cohen's Kappa scores for cross validation of annotations provided by 4 doctors (D1, D2, D3, D4). DA_DB is a cumulative score.

3.6 Final Dataset Composition

The final composition contains 5,450 high-resolution JPEG images across 8 top-level etiologic classes, 19 clinically meaningful subclasses, and 245 fine-grained disease labels. Each sample includes dense metadata: hierarchical disease labels, body parts, skin lesion descriptors, Fitzpatrick [7] and Monk skin tone [31] scores, diagnostic certainty, and image gradability. We consider 49 body parts and 47 lesion descriptors as concepts, which account for 96 unique concepts.
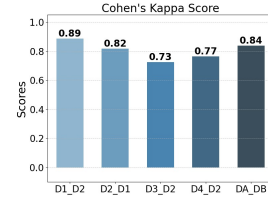
4 Dataset Overview and Statistics

Diagnostic structure and class granularity: DermaCon-IN is organized around an etiologically informed, clinically validated taxonomy rooted in Rook's [9] classification and aligned with ICD-11 [41]. The dataset includes 8 high-level diagnostic categories ranging from Infectious to Neoplastic, including No Definite Diagnosis — reflecting the full spectrum of dermatological conditions prevalent in South Asian outpatient settings [39]. These main classes are further expanded into 19 subclasses to capture hybrid and co-occurring disease states. For example, subclass combinations such as Inflammatory + Infectious (Bacterial) reflect polymorphic real-world presentations of superimposed two diseases. Each top-level category is populated with sufficient training instances for stratified benchmarking; notably, high-burden groups like fungal infections and eczema dominate in volume, while rare but clinically significant categories—e.g., keratinization disorders remain represented with enough density to enable few-shot generalization. The Disease label reflects 245 distinct disease types, which follow a long-tailed distribution with a **log-normal** fit to leaf-node frequencies, yielding an exponent of 1.8, as expected in real-world clinical settings. To better understand label

diversity in the dataset, refer Figure 4. This visualization underscores the need for imbalance-aware learning strategies.

Lesion Descriptor annotations: The visual descriptors of skin lesions annotated in DermaCon-IN follow an established dermatological vocabulary commonly used by clinicians to describe skin lesions in line with extant clinical literature [3]. Inspired by frameworks [5] previously validated in dermatology AI literature, we consulted board-certified dermatologists to select clinically meaningful descriptors aligned with disease patterns frequently encountered in Indian outpatient settings. Rather than assigning fixed concepts per disease category, each image was independently annotated, reflecting the realistic variability in lesion appearance across patients, body regions, and skin types. Statistical analysis in Figure 5 of concept-disease correlations validated this flexible annotation strategy that supports concept-supervised learning approaches. Details of Descriptors utilised for annotation are provided in Datasheet (Supplementary Material).
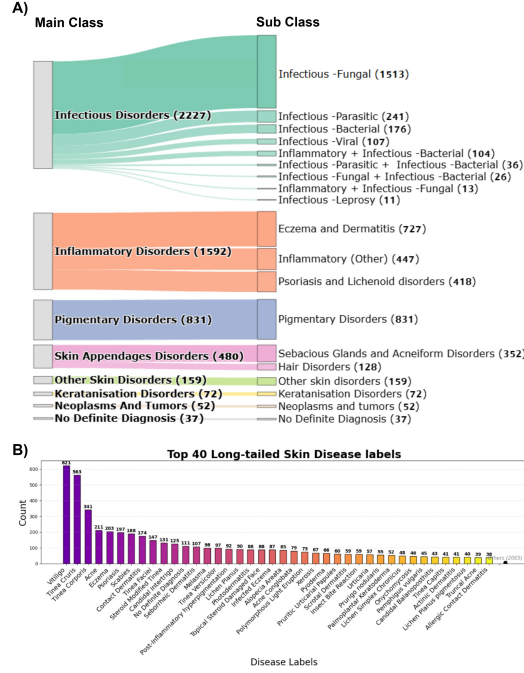

Figure 4: (A) Hierarchical structure of dermatological annotations (according to Rook's classification) showing main classes and their corresponding sub-classes with image counts (in bracket). (B) Distribution of the top 40 most frequent disease labels, illustrating the long-tailed nature of the dataset.

Anatomical Site annotations: We retain full views of affected anatomical regions wherever feasible. Partial cropping is applied in cases when identifiable facial features are present, in line with ethical guidelines to ensure patient privacy while preserving anatomical context reflecting how skin conditions are typically encountered in practice. This anatomical framing allows models to learn spatial priors: for instance, tinea capitis typically affects the scalp, while palmoplantar keratoderma appears on the palms and soles.

Such distributional cues are vital for accurate real-world diagnosis but are often lost in lesion-only images. Our dataset includes annotations for 49 distinct body sites, organized using both precise clinical terms and broader regional tags (e.g., trunk, extremities, scalp). A List of body parts annotated is provided in Datasheet (Supplementary Material).

Need for integration of Anatomical Context and Lesion Descriptors: Clinically, the same lesion type can indicate different diagnoses depending on its location; for example, a scaly plaque on the scalp might point to psoriasis, whereas a scaly plaque on the foot can suggest a fungal infection (tinea pedis). By jointly annotating lesion features (e.g., scales, plaques) and their anatomical context (e.g., scalp, foot), our dataset enables models to better reflect dermatologists' real-world diagnostic approach.
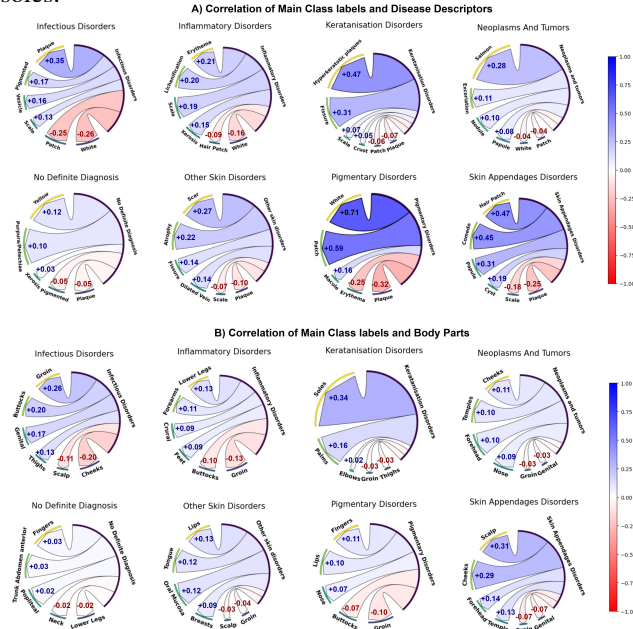

Figure 5: Chord diagrams depicting the most informative concept-class correlations for each main skin disease class. (A) Correlations between disease classes and clinical descriptors (e.g., morphology, texture, pigmentation); (B) correlations between disease classes and annotated body regions. For both, Pearson correlation coefficients were computed, and the top-k positive and bottom-k negative associations per class were selected. Ribbon widths represent correlation magnitude, and color encodes direction and strength (blue: positive, red: negative), highlighting characteristic clinical and anatomical patterns across disease groups.

Population structure and label density: The dataset reflects age and sex demographics typical of South Indian outpatient settings. The Dataset also adopts both Monk Skin Tone (MST) [31] and Fitzpatrick [7] scales, addressing the limitations of Fitzpatrick's UV-response bias. MST offers a perceptual alternative capturing wider tonal representation, especially for darker skin types, as the tonal scale has increased variation. The combined annotation aligns with Indian phenotypic distributions (MST 4–9, Fitzpatrick 3–4).

Statistical validation of concept and Anatomical coherence with Disease Labels: We examined Pearson correlation coefficients between (a) Disease descriptors and disease categories, and (b) anatomical body regions and disease categories, (refer Figure 5) to assess the biological plausibility and interpretability of our clinical annotations. These chord diagrams reveal statistically meaningful associations that align well with established dermatological knowledge. For instance, positive (high) correlations are observed between *erythema*, *vesicle*, and *scale* with inflammatory disorders, and between *hyperkeratotic plaques* and keratinisation disorders. Similarly, *white patches* and *pigmented lesions* show high positive associations with pigmentary and infectious disorders, respectively, underscoring the dermatologic specificity of the disease descriptors in general. Anatomical correlations further reinforce clinical fidelity. Keratinisation disorders predominantly localize to the *soles* and *palms*, consistent with plantar keratoderma patterns. Skin appendageal disorders, such as acne and seborrheic dermatitis, strongly associate with sebaceous-rich zones like the *scalp* and *cheeks* [3, 30]. These findings validate the anatomical tropisms encoded in the dataset.

5 Challenges, Opportunities & Limitations

The dataset presents a range of challenges and opportunities that stem from the inherent complexity of real-world clinical data, offering both practical constraints and avenues for robust model development:

Resolution heterogeneity: Images were cropped post-acquisition to remove garments and background clutter where feasible, though incidental artifacts (e.g., jewelry) remain in some cases. The resulting variability in resolution, arising from diverse capture devices and aspect ratios, is a natural outcome, but advantageous. It reflects real-world conditions, where patients may crop or capture images themselves, and encourages model robustness to such variations. Image heights range from 296 to 4,608 pixels and widths from 346 to 4,608 pixels, with

Figure 6: Resolution distribution of images in DermaCon-IN dataset

a mean resolution of 2,300x2,057 pixels. The average image area is 4.97M pixels ($\pm$3.01M), with an interquartile range of 2.62M–6.69M pixels (Figure 6), indicating consistently high-fidelity input for fine-grained modeling.
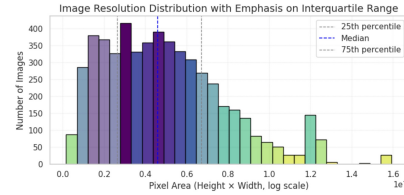
Hierarchical Labels and Clinical Distribution:

- **Class Imbalance:** Our hierarchical labelling across main and sub-classes reflects true outpatient frequencies, common conditions are well-represented, while others occur proportionally less. This mirrors real-world practice and enables models to learn from naturally occurring clinical distributions.
- **Long-tailed Disease Labels:** The dataset embraces the inherent long-tailed nature of dermatological diagnoses, where few diseases are prevalent and many are rare. This structure presents a valuable opportunity to train models that generalize across the full clinical spectrum, including rare disease categories.

Instance-level concepts: These concepts describe what is visually observed in each image, such as scaling and erythema, and introduce two key characteristics that make DermaCon-IN a rich dataset for advancing clinical AI:

- **Class-agnostic semantics:** Descriptors (used as concepts) are shared across classes and are not rigidly tied to any single diagnostic category (e.g., *scaling* alone ⤳ ichthyosis, whereas *scaling + erythema* ⤳ psoriasis), with diagnostic meaning arising from their combinations. This invites the development of models capable of compositional and context-aware reasoning.
- **Long-tailed distribution:** The natural skew in concept frequencies mirrors real-world prevalence, where rare but critical findings coexist with common patterns. This creates

Table 2: Performance benchmarking of the proposed dataset on the 8-main class diagnosis classification task, conducted using both CNN- and ViT-based standard architectures. All metrics are averaged over 5 random seeds.

Model	Pre-trained	Accuracy	Precision	Sensitivity	F1 Score
ResNet50 [13]	-	$47.45_{\pm 0.40}$	$46.59_{\pm 0.51}$	$47.44_{\pm 0.41}$	$46.43_{\pm 0.60}$
DenseNet121 [16]	-	$49.30_{\pm 0.30}$	$47.49_{\pm 0.86}$	$49.30_{\pm 0.29}$	$48.17_{\pm 0.74}$
ResNet50 [13]	ImageNet	$64.31_{\pm 0.22}$	$63.41_{\pm 0.29}$	$64.31_{\pm 0.23}$	$63.31_{\pm 0.25}$
DenseNet121 [16]	ImageNet	$65.20_{\pm 0.48}$	$64.62_{\pm 0.48}$	$65.20_{\pm 0.48}$	$64.37_{\pm 0.35}$
EffNet-B4_b4 [35]	ImageNet	$64.28_{\pm 0.34}$	$63.53_{\pm 0.64}$	$64.27_{\pm 0.34}$	$63.38_{\pm 0.39}$
ViT-B/16-224 [6]	ImageNet	$64.09_{\pm 1.03}$	$62.59_{\pm 1.03}$	$62.88_{\pm 1.67}$	$62.98_{\pm 1.02}$
ViT-B/16-384 [6]	ImageNet	$66.95_{\pm 0.19}$	$65.39_{\pm 0.13}$	$66.95_{\pm 0.20}$	$65.78_{\pm 0.06}$
MaxViT-B/512 [38]	ImageNet	$66.92_{\pm 0.48}$	$66.30_{\pm 0.80}$	$66.92_{\pm 0.48}$	$65.90_{\pm 0.73}$
Swin-B/4W12-384 [24]	ImageNet	$\mathbf{70.41_{\pm 0.41}}$	$\mathbf{69.83_{\pm 0.37}}$	$\mathbf{70.41_{\pm 0.42}}$	$\mathbf{69.69_{\pm 0.46}}$

Table 3: Performance comparison of model variants using the `Swin-B/4W12-384` backbone. The first two rows are baselines without a concept bottleneck (CB) layer, used for 8-main class (MC) and 19-subclass (SC) classification. The next four rows report CBMs trained with different concept sets: lesion descriptors (47), body parts (49), and both (96). The last merged rows present individual layer (SC & MC) performance of a Hierarchical CBM (Type 1 & 2) combining the CB layer with joint SC and MC classification as described in Fig 7. All metrics are results of end-to-end training and are averaged over 5 random seeds.

Classification head	Concepts	Accuracy	Precision	Sensitivity	F1 Score	Macro AUC
MC	-	$\mathbf{70.41_{\pm 0.41}}$	$\mathbf{69.83_{\pm 0.37}}$	$\mathbf{70.41_{\pm 0.42}}$	$\mathbf{69.69_{\pm 0.46}}$	$\mathbf{78.51_{\pm 0.59}}$
SC	-	$58.27_{\pm 0.22}$	$56.64_{\pm 0.45}$	$58.27_{\pm 0.22}$	$56.81_{\pm 0.43}$	$83.11_{\pm 2.55}$
(CBM-D) Concepts + MC	Descriptors	$68.57_{\pm 0.72}$	$67.63_{\pm 0.97}$	$68.55_{\pm 0.72}$	$67.69_{\pm 79.48}$	$85.18_{\pm 2.98}$
(CBM-B) Concepts + MC	Body parts	$68.38_{\pm 0.31}$	$67.69_{\pm 0.51}$	$68.31_{\pm 0.27}$	$67.90_{\pm 0.26}$	$84.96_{\pm 1.27}$
Concepts + MC	Descriptors & Body parts	$68.12_{\pm 0.43}$	$67.69_{\pm 0.71}$	$68.10_{\pm 0.48}$	$67.56_{\pm 0.48}$	$82.78_{\pm 2.70}$
Concepts + SC	Descriptors & Body parts	$55.54_{\pm 0.73}$	$56.85_{\pm 0.92}$	$55.53_{\pm 0.76}$	$55.75_{\pm 0.85}$	$79.42_{\pm 0.17}$
(Type1) Concepts + SC	Descriptors & Body parts	$53.98_{\pm 0.40}$	$56.12_{\pm 0.74}$	$53.98_{\pm 0.39}$	$54.49_{\pm 0.66}$	$76.13_{\pm 1.52}$
+ MC		$67.78_{\pm 0.47}$	$67.32_{\pm 0.67}$	$67.66_{\pm 0.48}$	$66.92_{\pm 0.37}$	$79.53_{\pm 0.62}$
(Type 2) Concepts + SC	Descriptors & Body parts	$56.11_{\pm 0.67}$	$55.49_{\pm 0.0.62}$	$56.09_{\pm 0.9}$	$54.49_{\pm 0.66}$	$76.13_{\pm 1.52}$
+ MC		$69.90_{\pm 0.20}$	$68.82_{\pm 0.36}$	$69.89_{\pm 0.19}$	$69.08_{\pm 0.31}$	$77.01_{\pm 2.24}$

opportunities to tackle challenges in multi-concept learning and rare concept detection— core problems in clinical AI.

Limitations. In accordance with ethical considerations, all images were anonymised by masking identifiable facial features, such as the eyes, and cropping facial regions where necessary. While essential for protecting patient identity, this may limit the model's ability to accurately learn or detect diseases that primarily manifest on the face.

6 Benchmarking with Models

6.1 Standard architectures

DermaCon-IN comprises high-resolution clinical photographs with multiple co-occurring lesions, varied anatomical regions, and hierarchically structured multi-label annotations. We selected architectures based on their complementary modelling strengths to benchmark model performance under these conditions. Convolutional neural networks such as ResNet50 [13], DenseNet121 [16], and EfficientNet (`EffNet-B4_b4`) [35] are effective in capturing localized texture patterns and edge-level features, owing to their convolutional inductive biases and limited receptive fields. To complement this, we incorporated Vision Transformer (ViT) architectures [6], which leverage self-attention to relate spatially distant regions within an image. The ViT variants evaluated includes ViT-Base (`ViT-B/16-224` [6], `ViT-B/16-384`) [6], MaxViT-Base (`MaxViT-B/512`) [38], and Swin-Base (`Swin-B/4W12-384`) [24]. Among these, the Swin Transformer consistently achieved the best results for Main class prediction across evaluation metrics, demonstrating improved handling of both multi-class classification and class imbalance. Table 2 summarizes the performance of all models considered. Swin Transformer's shifted window mechanism enables efficient modeling of non-contiguous regions, while its hierarchical representation captures both fine-grained lesion details and broader spatial patterns. These traits align closely with our dataset. We believe this alignment contributed to Swin's better performance.

Based on these observations, we adapted the `Swin-B/4W12-384` [24] variant of the Swin Transformer as the backbone for subsequent analysis and in concept bottleneck models (CBMs) [22] as shown in Table 3. The model was initialized with weights pretrained on ImageNet-22k and fine-tuned end-to-end on our dataset. Input images were resized and padded to 512×512 for further

classification. We performed a stratified, subject-wise 80:20 split over Sub Class and reported all the results with the same split. We adapted weighted sampling strategies to handle class imbalance, and details of which are discussed in Supplementary Sec. B.

6.2 Concept Bottleneck Modeling for Interpretablity

Architecture. Given an input image x, the Swin-Transformer encoder E_θ yields a latent representation $z = E_\theta(x)$. A linear projection maps z to *concept logits* $c^\ell \in \mathbb{R}^{B+D}$, which are then passed through a sigmoid activation to obtain the interpretable *concept vector* $c = [c^{bp}, c^{ld}] = \sigma(c^\ell) \in [0,1]^{B+D}$, where c^{bp} denotes B **body-part** concepts and c^{ld} denotes D **lesion-descriptor** concepts. While both c and c^ℓ is used for interpretability and concept supervision, the downstream classifier f operates on the concept logits c^ℓ to produce task logits $y = f(c^\ell)$, predicting either a *Main-Class* (MC) or *Sub-Class* (SC) label. This architecture is presented in Figure 7(A).

Concept ablation and joint–stream effects. To quantify the contribution of each concept group we trained two ablated models: **CBM-D**, which keeps only lesion-descriptor concepts c^{ld}, and **CBM-B**, which keeps only body-part concepts c^{bp}, both predicting MC labels. Each single–stream variant retained high accuracy (Table. 2) demonstrating that the two concept families are independently learnable.

Figure 7: Architectural setup of Concept-bottleneck models for Main class (MC) and Sub class (SC) classification

By contrast, the *full* CBM represents the true clinical diagnostic fidelity, in which both c^{bp} and c^{ld} co-exist in the bottleneck, achieved performance comparable to the individual concept streams, but revealed a systematic imbalance in activation: In many samples, only one concept group (typically descriptors) fired strongly, whereas the other (body parts) was under-activated (Fig. 8, bottom row). This led to a modest but consistent drop in overall accuracy, pointing to a *representational bottleneck* whereby competition for limited capacity biases the model toward a single semantic stream. These observations emphasise the need for improved multi-concept learning mechanisms that can balance several concept families simultaneously.
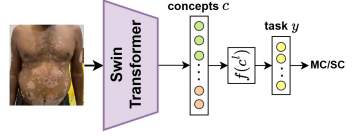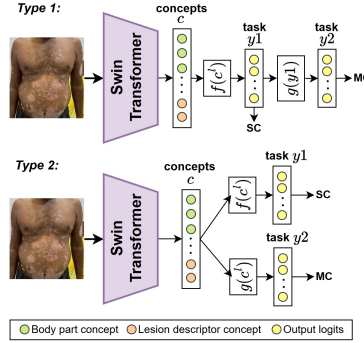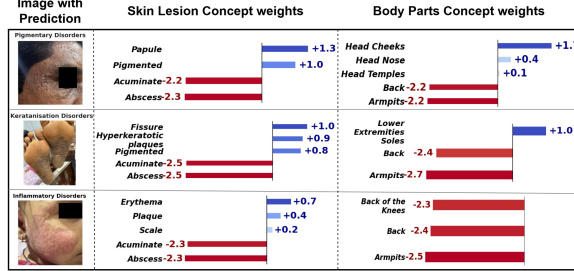

Figure 8: Bar plot of top and bottom-k contributing concepts (lesion descriptors and body parts) for the model's prediction. Contributions are shown as signed log-scaled weights derived from the CBM's intermediate logits.

Hierarchical CBMs. We explore two designs for joint SC–MC prediction (Figure. 7(B)):

1. **Type 1 — cascade.** Concepts first predict sub-classes via $y1 = f(c)$; these logits are then mapped to main classes through a second head $y2 = g(y1)$, ensuring taxonomy consistency by construction.
2. **Type 2 — parallel.** Both SC and MC are predicted from the shared concept vector through independent heads, $y1 = f(c)$ and $y2 = g(c)$, leveraging multi-task learning for implicit regularization.

Empirically, the *parallel* configuration surpassed the *cascade* alternative across all evaluation metrics (Table. 2), likely due to effective regularization and information sharing through the multi-task learning setup.

Qualitative Analysis. To validate the spatial grounding of concepts, we employed Grad-CAM visualizations over Swin ViT on specific concept heads (Figure 9). For each selected concept (from both descriptor and body part categories), we backpropagated gra-
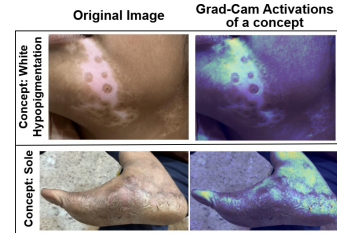

Figure 9: Examples of Grad-cam visualizations over Swin Transformer by choosing a specific concept with the best CBM model (Type-2).

8

dients from the concept prediction to the image space, producing activation heatmaps. These visualizations confirmed that the model's concept activations were often localized to semantically and anatomically appropriate regions, supporting the faithfulness of the learned representations.

To further assess whether the model's predictions are semantically grounded, we evaluate the alignment between its learned class-concept weights (MC branch of Type-2) and the statistical relevance (Pearson correlation, Section 4) of each concept to the class labels in the dataset (Figure 10). Alignment varies notably across diagnostic categories. *Pigmentary Disorders* and *Keratinisation Disorders* show strong Spearman correlations and statistically significant p-values ($p < 0.05$), suggesting that the model reliably prioritizes clinically meaningful features for these classes. In contrast, *Neoplasms and Tumors* show weak or negative alignment, indicating reliance on non-semantic or latent cues, possibly due to low representation in the dataset. Whereas, *No Definite Diagnosis* shows negative correlations as desired. Classes like *Skin Appendageal Disorders, etc.* exhibit partial alignment.
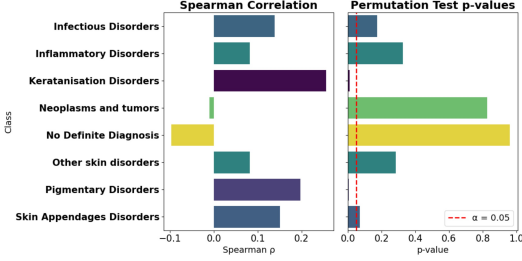
Figure 10: Class-wise assessment of alignment between the model's learned label weights over concepts and the dataset-derived correlation of concepts with class labels. The Spearman correlation measures the rank agreement between model-assigned concept importance and empirical concept–class correlations. Permutation test p-values (based on Pearson correlation) assess the statistical significance of this alignment.

Overall, these findings highlight that while the model is capable of learning semantically meaningful representations in some contexts, its reliance on concept supervision is uneven and class-dependent. This motivates future work in enforcing more robust concept–class alignment, particularly for clinically ambiguous or visually heterogeneous disease categories.

7   Conclusion and Future Directions.

 DermaCon-IN captures real-world dermatological presentations from the South Indian population, offering concept-level annotations such as body parts and disease descriptors. It addresses gaps in skin tone diversity and regional disease patterns, serving both as a region-specific benchmark and a valuable addition to global dermatological datasets. By enabling evaluation beyond labels, it supports clinically grounded, interpretable learning—a step closer towards clinical deployment.

Targeted future work. Our findings point to several *method-driven* avenues for closing the identified gaps. These steps can help models to not only classify accurately but also reason in clinically meaningful ways.They are as follows:

- **Concept-weight normalisation:** adding explicit regularisers that penalise disproportionate reliance on a single concept group, encouraging balanced gradient flow.

- **Hierarchy-consistent objectives:** coupling the SC and MC heads with cross-level consistency losses to discourage contradictory evidence pathways.

- **Curriculum and re-sampling strategies:** oversampling under-represented concept combinations (e.g. body-part signals within neoplasm classes) to equalise learning pressure across concept space.

Broader integration. Because DermaCon-IN offers strong coverage of South-Indian skin tones and disease spectra, its concept annotations complement existing global datasets. Merging these resources will enable training of larger, more broadly representative models—paving the way toward a unified *foundation-level* representation for dermatological imaging.

Ethical Clearance Statement: The dataset was collected in accordance with institutional ethical guidelines and has been approved by the Institute Ethics Committee of the Indian Institute of Technology Hyderabad under protocol number *IITH/IEC/2025/01/05*.

Implementation: The experiments were run on 4 GPUs of Nvidia-A6000, each of 42GB RAM. The dataset sizes around ~ 4 GB. The code used in this work is available at GitHub.

Availability and Licensing: The dataset can be downloaded at Harvard Dataverse. This work is licensed under CC BY-NC-SA 4.0. To view a copy of this license, visit creativecommons.org.

References

[1] N. Alipour et al. Skin type diversity in skin lesion datasets: A review. *International Journal of Dermatology*, 63:198–210, 2024. doi:10.1007/s13671-024-00440-0.

[2] P. Balasubramanian et al. Epidemiological study of skin disorders in andaman and nicobar islands. *Indian Journal of Dermatology*, 66(5):454–458, 2021. doi:10.4103/ijd.IJD_30_20.

[3] Jean L. Bolognia, Julie V. Schaffer, and Lorenzo Cerroni. *Dermatology*. Elsevier, 4 edition, 2017. ISBN 9780702062759.

[4] R. Daneshjou et al. Disparities in dermatology ai performance on a diverse, curated clinical image set. *Scientific Reports*, 12:12565, 2022. doi:10.1126/sciadv.abq6147.

[5] R. Daneshjou et al. Skincon: A skin disease dataset densely annotated by domain experts for fine-grained debugging and analysis. In *Advances in Neural Information Processing Systems (NeurIPS), Datasets and Benchmarks Track*, 2022. URL `https://proceedings.neurips.cc/paper_files/paper/2022/hash/7318b51b52078e3af28197e725f5068a-Abstract-Datasets_and_Benchmarks.html`.

[6] Alexey Dosovitskiy et al. An image is worth 16x16 words: Transformers for image recognition at scale. In *International Conference on Learning Representations (ICLR)*, 2021.

[7] Thomas B. Fitzpatrick. Soleil et peau. *Journal de Médecine Esthétique*, 2:33–34, 1975.

[8] P. Gottfrois et al. Passion for dermatology: Bridging the diversity gap with pigmented skin images from sub-saharan africa. In *Medical Image Computing and Computer Assisted Intervention – MICCAI 2024*, pages 703–712. Springer Nature Switzerland, 2024.

[9] Christopher E.M. Griffiths et al. *Rook's Textbook of Dermatology*. Wiley-Blackwell, 10 edition, 2024. ISBN 9781119709213. URL `https://www.wiley.com/en-us/Rook%27s%2BTextbook%2Bof%2BDermatology%2C%2B4%2BVolume%2BSet%2C%2B10th%2BEdition-p-00402062`. 4-volume set.

[10] M. Groh et al. Evaluating deep neural networks trained on clinical images in dermatology with the fitzpatrick 17k dataset. In *Proceedings of the IEEE/CVF Conference on Computer Vision and Pattern Recognition (CVPR)*, pages 1820–1828, 2021.

[11] Robert J Hay, Neil E Johns, Hannah C Williams, and et al. The global burden of skin disease in 2010: An analysis from the global burden of disease study 2010. *The Journal of Investigative Dermatology*, 134(6):1527–1534, 2014. doi:10.1038/jid.2013.446.

[12] Roderick J. Hay et al. Skin disease in the tropics and the lessons that can be learned from leprosy and other neglected diseases. *Acta Dermato-Venereologica*, 100:adv00113, 2020. doi:10.2340/00015555-3469.

[13] Kaiming He et al. Deep residual learning for image recognition. In *Proceedings of the IEEE Conference on Computer Vision and Pattern Recognition (CVPR)*, pages 770–778, 2016.

[14] C. Hernández et al. Bcn20000: Dermoscopic lesions in the wild. *Scientific Data*, 11:641, 2024. doi:10.1038/s41597-024-03387-w.

[15] Pengcheng Huai et al. Global burden of skin and subcutaneous diseases: an update from the global burden of disease study 2021. *British Journal of Dermatology*, ljaf071, 2025. doi:10.1093/bjd/ljaf071. Published: 11 April 2025.

[16] Gao Huang et al. Densely connected convolutional networks. In *Proceedings of the IEEE Conference on Computer Vision and Pattern Recognition (CVPR)*, pages 4700–4708, 2017.

[17] ISIC. Siim-isic 2020 challenge dataset, 2020. URL `https://doi.org/10.34970/2020-ds01`. Creative Commons Attribution-Non Commercial 4.0 International License.

[18] N. S. Jayanthi et al. Epidemiological pattern of skin diseases among patients attending dermatological outpatient department at a tertiary care centre, north chennai. *Indian Journal of Clinical and Experimental Dermatology*, 3(4):134–137, 2017. doi:10.18231/2455-6769.2017.0032.

[19] Emily Johnson and Robert Lee. Global burden of skin diseases in 2019: Updated estimates from the global burden of disease study 2019. *The Lancet Global Health*, 8(11):e1539–e1540, 2020. doi:10.1016/S2214-109X(20)30386-7.

[20] C. Karimkhani et al. Global skin disease morbidity and mortality: An update from the global burden of disease study 2013. *JAMA Dermatology*, 153(5):406–412, 2017. doi:10.1001/jamadermatol.2016.5538.

[21] J. Kawahara, S. Daneshvar, G. Argenziano, and G. Hamarneh. 7-point checklist and skin lesion classification using multi-task multi-modal neural nets. *IEEE Journal of Biomedical and Health Informatics*, Apr 2018. doi:10.1109/JBHI.2018.2824327. Epub ahead of print.

[22] Pang Wei Koh et al. Concept bottleneck models. In *Proceedings of the 37th International Conference on Machine Learning*, volume 119, pages 5338–5348, 2020.

[23] Melissa R. Laughter, Mayra B. C. Maymone, Chante Karimkhani, Chandler Rundle, Sophia Hu, Sophia Wolfe, Katrina Abuabara, Parker Hollingsworth, Gil S. Weintraub, Cory A. Dunnick, Adnan Kisa, Giovanni Damiani, Aziz Sheikh, Jasvinder A. Singh, Takeshi Fukumoto, Rupak Desai, Ayman Grada, Irina Filip, Amir Radfar, Mohsen Naghavi, and Robert P. Dellavalle. The burden of skin and subcutaneous diseases in the united states from 1990 to 2017. *JAMA Dermatology*, 156(8): 874–881, 2020. doi:10.1001/jamadermatol.2020.1573. URL https://jamanetwork.com/journals/jamadermatology/fullarticle/2767074.

[24] Ze Liu et al. Swin transformer: Hierarchical vision transformer using shifted windows. In *Proceedings of the IEEE/CVF International Conference on Computer Vision (ICCV)*, pages 10012–10022, 2021.

[25] M. López-Pérez et al. Are generative models fair? a study of racial bias in dermatological image generation, 2025. URL https://arxiv.org/abs/2501.11752.

[26] T. Mendonça et al. Ph²: A dermoscopic image database for research and benchmarking. In *Proceedings of the 35th International Conference of the IEEE Engineering in Medicine and Biology Society (EMBC)*, Osaka, Japan, July 2013.

[27] A. O'Malley et al. Ensuring appropriate representation in artificial intelligence–generated medical imagery: Protocol for a methodological approach to address skin tone bias. *JMIR AI*, 3:e58275, 2024. doi:10.2196/58275. URL https://ai.jmir.org/2024/1/e58275.

[28] A. G. C. Pacheco et al. Pad-ufes-20: A skin lesion dataset composed of patient data and clinical images collected from smartphones. *Data in Brief*, 32:106221, 2020. doi:10.1016/j.dib.2020.106221.

[29] Adam Paszke et al. Pytorch: An imperative style, high-performance deep learning library. https://github.com/pytorch/pytorch, 2019.

[30] Ronald P. Rapini. *Dermatology: 2-Volume Set*. Mosby, 1 edition, 2007. ISBN 9780721601573.

[31] Candice Schumann, Femi Olanubi, Auriel Wright, Ellis Monk, Courtney Heldreth, and Susanna Ricco. Consensus and subjectivity of skin tone annotation for ml fairness. In *Advances in Neural Information Processing Systems 36 (NeurIPS 2023), Datasets and Benchmarks Track*, 2023. URL https://proceedings.neurips.cc/paper_files/paper/2023/hash/60d25b3210c92f5ba2002a8e1f1adf1c-Abstract-Datasets_and_Benchmarks.html.

[32] B. Shah et al. Epidemiological study of skin diseases in himatnagar. *International Journal of Research in Dermatology*, 5(2):342–345, 2019. doi:10.18203/issn.2455-4529.IntJResDermatol20190453.

[33] X. Sun et al. A benchmark for automatic visual classification of clinical skin disease images. In B. Leibe, J. Matas, N. Sebe, and M. Welling, editors, *Computer Vision – ECCV 2016*, volume 9910 of *Lecture Notes in Computer Science*, pages 206–222. Springer, Cham, 2016. doi:10.1007/978-3-319-46466-4_13.

[34] M. D. Szeto et al. Dermatologic data from the global burden of disease study 2019 and the patientslikeme online support community: Comparative analysis. *JMIR Dermatology*, 7:e50449, 2024. doi:10.2196/50449. URL https://pubmed.ncbi.nlm.nih.gov/39661989/.

[35] Mingxing Tan et al. Efficientnet: Rethinking model scaling for convolutional neural networks. In *Proceedings of the 37th International Conference on Machine Learning (ICML)*, pages 6105–6114. PMLR, 2020.

[36] K. J. S. Thakur et al. The burden of skin diseases in india: Global burden of disease study 2017. *Indian Journal of Dermatology, Venereology and Leprology*, 87(6):764–771, 2021. doi:10.25259/IJDVL_978_20.

[37] P. Tschandl et al. The ham10000 dataset, a large collection of multi-source dermatoscopic images of common pigmented skin lesions. *Scientific Data*, 5:180161, 2018. doi:10.1038/sdata.2018.161. URL `https://doi.org/10.1038/sdata.2018.161`.

[38] Zihang Tu et al. Maxvit: Multi-axis vision transformer. In *European Conference on Computer Vision (ECCV)*, 2022.

[39] Katelyn Urban et al. The global, regional, and national burden of fungal skin diseases in 195 countries and territories: A cross-sectional analysis from the global burden of disease study 2017. *JAAD International*, 2:22–27, 2021. doi:10.1016/j.jdin.2020.10.003.

[40] A. Ward et al. Creating an empirical dermatology dataset through crowdsourcing with web search advertisements. *JAMA Network Open*, 7(11):e2446615, November 2024. doi:10.1001/jamanetworkopen.2024.46615.

[41] World Health Organization. *International Classification of Diseases, 11th Revision (ICD-11)*, 2019. URL `https://icd.who.int/`. Adopted by the 72nd World Health Assembly in 2019; came into effect on 1 January 2022.

[42] Aobuliaximu Yakupu et al. The burden of skin and subcutaneous diseases: findings from the global burden of disease study 2019. *Frontiers in Public Health*, 11:1145513, 2023. doi:10.3389/fpubh.2023.1145513.

[43] A. Yilmaz et al. Derm12345: A large, multisource dermatoscopic skin lesion dataset with 40 subclasses. *Scientific Data*, 11(1):1302, November 2024. doi:10.1038/s41597-024-04104-3.

Supplementary Material for DermaCon-IN

A Dataset Details

A.1 Rook's Classification for a Hierarchical Framework

Most dermatology datasets, such as *SD-198* [33]and *SCIN* [40], employ flat diagnostic label structures without an overarching clinical taxonomy. Others, like *Fitzpatrick17k* [10] and *SkinCon* [5], offer fine-grained or concept-level annotations but do not embed these within an etiologically structured or pathophysiology-aware hierarchy. As a result, they fall short of modeling the layered reasoning typical of clinical diagnosis. While sufficient for benchmarking classification models, these taxonomies lack clinical depth and fail to represent the structured reasoning used in dermatological diagnosis.

Clinical Relevance: Rook's taxonomy [9] introduces a hierarchical framework grounded in disease etiology and pathological processes, organizing conditions into superclasses such as *infectious*, *inflammatory*, *pigmentary*, and *appendageal*, etc. This mirrors how clinicians formulate differential diagnoses from broad mechanisms to specific entities and enables AI systems to produce outputs that resonate with clinical logic.

Contextual Suitability: In Indian outpatient dermatology, where fungal, pigmentary, and inflammatory conditions predominate, this structure offers strong alignment with real-world case loads. Unlike neoplasm-focused Western datasets, Rook's [9] schema reflects the diversity and prevalence of diseases encountered in Low & Middle Income Countries (LMIC) settings, while remaining extensible to global contexts.

Curation and Learning Advantages: A hierarchical setup facilitates consistent labeling, balanced representation across superclasses, and structured sampling strategies. It also supports coarse-to-fine prediction models, multi-task learning, and scalable dataset expansion.

Interoperability with Clinical Systems: Crucially, Rook's classification aligns with international standards such as the WHO's ICD-10 [41] and ICD-11, which also structure diseases by etiology and anatomical relevance. Since ICD codes underpin electronic health records, billing, and decision support tools, adopting a Rook-aligned hierarchy ensures that the dataset remains interoperable with clinical infrastructures. This enables seamless integration into healthcare workflows, extending its utility well beyond academic modeling to real-world deployment.

A.2 Descriptor Design and Clinical Alignment

Descriptor Design and Selection: We annotate 5,450 dermatological images using 47 carefully selected descriptors encompassing primary lesions, secondary changes, pigmentary alterations, vascular anomalies, and surface/nail abnormalities. The taxonomy is rooted in established dermatological frameworks [3], ensuring clinical interpretability and consistency with medical curricula and diagnostic practice. While many descriptors overlap with those used in SkinCon [5] (e.g., *papule*, *plaque*, *vesicle*), our set incorporates necessary refinements based on regional prevalence and diagnostic relevance. Descriptors with high clinical utility but low frequency (e.g., *poikiloderma*, *gray*, *salmon*) were retained to preserve diagnostic granularity. The descriptors such as *translucent*, *friable*, and *dome-shaped* lacked distinct visual features in $2D$ clinical images and so were not included in the list of descriptors, which were otherwise part of SkinCon descriptors.

Contextual Tailoring for Indian Dermatology: Our descriptor set is designed with sensitivity to Indian outpatient dermatology. Conditions such as vitiligo and post-inflammatory hyperpigmentation necessitate precise pigmentary annotations (*white*, *gray*, *brown*, *pigmented*). Similarly, endemic infections (e.g., scabies, impetigo) justify the inclusion of *crust*, *burrow*, and *abscess*. Chronic inflammatory presentations (*lichenification*, *hyperkeratotic plaques*) and nail findings (*pitted nail*, *discolored nail*) are also integrated based on their diagnostic frequency and clinical relevance in South Asia.

Standardization and Future Compatibility: Despite its regional grounding, our descriptor vocabulary remains aligned with global dermatological standards, enabling seamless integration with future datasets developed under similar clinically guided frameworks. By leveraging literature-backed terminology, our schema offers both backward compatibility with existing datasets like Skin-Con [5] and forward compatibility with evolving multimodal dermatology benchmarks.

Summary. Our descriptor design balances regional specificity with standardization. It enhances diagnostic interpretability, improves label quality for model training, and facilitates interoperability across future dermatological datasets. A detailed table of descriptors, definitions, and rationale is provided in Sup. Table 4.

Table 4: Complete Concept Descriptor Table with Definitions and Reasoning.

S.No	Concept	Explanation	Reason for Choosing the Descriptor
1	Abscess	A localized collection of pus within the dermis or subcutaneous tissue, typically surrounded by inflamed tissue; clinically presents as a painful, erythematous, fluctuant nodule.	Common in bacterial infections; present frequently in tropical and humid climates.
2	Acuminate	A lesion with a tapering, pointed shape; commonly seen in viral warts.	Seen in viral warts and common sexually transmitted infections like condyloma in Indian OPDs.
3	Atrophy	A reduction or thinning of tissue, which may involve the epidermal (outer skin layer), dermal (middle layer), or subcutaneous (deep fat and connective tissue layer).	Frequently observed in chronic corticosteroid use and dermatoses like lichen sclerosus.
4	Brown (Hyperpigmentation)	Darkened area of the skin due to excess melanin.	Extremely common in post-inflammatory states and melasma in the Indian population.
5	Bulla	A circumscribed lesion > 1 cm in diameter that contains liquid (clear, serous or haemorrhagic).	Seen in autoimmune and infective blistering disorders; important in differential diagnosis.
6	Burrow	It is a thin, wavy, slightly raised line on the skin, typically found between the fingers or toes, caused by the scabies mite burrowing under the surface.	Highly relevant in scabies, which has significant endemic prevalence in India.
7	Comedo	Comedo is a blocked skin pore caused by the accumulation of oil and dead skin cells. An open comedo, commonly known as a blackhead, has an exposed surface where the trapped material darkens due to air exposure. A closed comedo, or whitehead, remains sealed under the skin, forming a small bump.	Key feature in acne, a major dermatological complaint in adolescents and young adults.
8	Crust	Dried serum, blood or pus on the surface of the skin.	Present in infected eczemas and impetigo, common in Indian children.
9	Cyst	Cyst is a papule or nodule that contains fluid or semi-fluid material, making it soft and fluctuant to touch.	Frequent presentation in both cosmetic and inflammatory conditions, like epidermoid cysts.
10	Dilated Vein	Enlarged, visible superficial vein; may be seen in varicosities or venous insufficiency.	Observed in varicose conditions and vascular anomalies, especially in rural patients.
11	Discolored Nail	Alteration in nail color due to trauma, infection, pigmentation, or systemic disease.	Indicator of systemic illness, fungal infections, or trauma-related disorders.
12	Edema	Swelling of the skin due to fluid accumulation in the dermis or subcutaneous tissue.	Secondary signs in infections, inflammatory conditions, and systemic diseases.
13	Erosion	Superficial loss of the epidermis, often due to ruptured blisters; heals without scarring.	Occurs in healing blisters and vesiculobullous diseases seen in Indian settings.
14	Erythema	Redness of the skin due to increased blood supply.	Fundamental indicator of inflammation; often subtle in pigmented skin.
15	Excoriation	A loss of the epidermis and a portion of the dermis due to scratching or an exogenous injury.	Seen in pruritic disorders like scabies, atopic dermatitis, and lichen simplex chronicus.
16	Exophytic/Fungating	It describes a type of lesion that grows rapidly, breaks through the skin surface, and often appears ulcerated, foul-smelling, and infected, resembling a fungus-like mass.	Helps classify malignant and advanced skin lesions; relevant in tertiary care.
17	Exudate	Oozing fluid composed of serum, pus, or blood; typically due to inflammation or infection.	Observed in infected wounds, ulcers, and pyodermas.

Table 4 (continued): Complete Concept Descriptor Table

S.No	Concept	Explanation	Reason for Choosing the Descriptor
18	Fissure	Fissure is a linear crack or break in the skin that begins in the outermost layer (stratum corneum) and may extend into the deeper dermis, often causing pain or bleeding.	Very common in xerotic skin conditions and hand/foot eczema exacerbated by occupational exposure.
19	Flat-topped	Lesion with a flattened horizontal surface; characteristic of lichen planus.	Key for diagnosing lichen planus, prevalent in Indian adults.
20	Gray	A color descriptor typically indicating post-inflammatory hyperpigmentation or pigment incontinence.	Represents pigment incontinence or deeper melanin deposition; seen in pigmented disorders.
21	Hair Patch	Hair patch refers to a localized area on the skin where hair is either abnormally present (increased density or unusual location) or absent (loss of hair in a defined area)	Helps identify abnormal loss or growth of hair in a specific area.
22	Hyperkeratotic plaques	Thickened plaques with an excessive build-up of keratin.	Observed in psoriasis, lichen simplex, and chronic eczema, common in Indian clinics.
23	Induration	It refers to an area of the skin or tissue that feels firm or hardened to the touch, without any underlying calcification or bone formation.	Helps differentiate infections (e.g., cellulitis) or granulomatous conditions (e.g., leprosy).
24	Lichenification	It is thickened, rough skin with exaggerated skin lines, typically resulting from repeated rubbing or scratching	Common in chronic atopic and lichen simplex; consequence of habitual scratching.
25	Macule	A flat, circumscribed, nonpalpable lesion that differs in colour from the surrounding skin.	Key to diagnosing pigmentary and vascular disorders like vitiligo and leprosy.
26	Nodule	An elevated, solid, palpable lesion > 1 cm usually located primarily in the dermis and/or subcutis.	Important for deep fungal infections, cutaneous TB, or cystic swellings in endemic areas.
27	Papule	An elevated, solid, palpable lesion that is $\leq$ 1 cm in diameter.	Seen in common dermatoses like folliculitis, acne, and viral warts.
28	Patch	A large area of colour change, with a smooth surface.	Central to identifying vitiligo, pityriasis alba, and leprosy.
29	Pedunculated	Lesion attached by a narrow stalk.	Helps in the classification of benign tumors like acrochordons or neurofibromas.
30	Pigmented	Lesions exhibiting increased pigment; may be brown, gray, or black.	Essential in differentiating dermatoses on brown skin; pigmentary presentations dominate.
31	Pitted Nail	Small depressions on the nail surface.	Common signs of nail psoriasis and alopecia areata.
32	Plaque	A circumscribed, palpable lesion $\geq$ 1 cm in diameter; most plaques are elevated.	Describes major lesion morphology in tinea, psoriasis, and lichen simplex.
33	Poikiloderma	Simultaneous presence of atrophy, telangiectasia and hypo and hyperpigmentation.	Seen in late-stage connective tissue diseases; needs documentation in atypical Indian cases.
34	Purpura/Petechiae	Haemorrhage into the skin due to pathological processes, primarily of blood vessels.	Observed in vasculitis and hematological disorders.
35	Pustule	A circumscribed lesion that contains pus.	Seen in acne, folliculitis, and impetigo; frequently present in outpatient cases.
36	Salmon	Pink-orange hue used to describe psoriatic lesions, especially on lighter skin tones.	Color reference for certain psoriatic plaques in lighter Indian skin tones.
37	Scale	A visible accumulation of keratin, forming a flat plate or flake.	Typical in dermatophytosis, psoriasis, and seborrheic dermatitis; common in humid climates.
38	Scar	Fibrotic replacement of normal skin architecture after injury.	Important to track disease healing and secondary changes post-injury or intervention.
39	Striae	Linear atrophic lesions due to dermal tearing.	Common due to corticosteroid use, obesity, puberty, and pregnancy-related changes.
40	Telangiectasia	Permanently dilated capillaries.	Seen in rosacea, lupus, and long-term corticosteroid use.
41	Ulcer	Full-thickness loss of the epidermis plus at least a portion of the dermis.	Crucial for identifying diabetic foot, leprosy, and chronic venous ulcers.
42	Vesicle	A circumscribed lesion $\leq$ 1 cm in diameter that contains liquid (clear, serous or haemorrhagic).	Key feature in varicella, dermatitis herpetiformis, and contact dermatitis.
43	Warty	Verrucous surface resembling a wart; rough and irregular.	Descriptive of HPV-induced lesions and seborrheic keratoses, which are common in the elderly in India.
44	Wheal	A transient elevation of the skin due to dermal edema.	Seen in urticaria due to infections, drugs, and food reactions.
45	White (Hypopigmentation)	Lighter than normal skin color due to loss or reduction of melanin.	Central to vitiligo, pityriasis alba, and tinea versicolor which are frequent in India.
46	Xerosis	Abnormal dryness of the skin.	Highly prevalent due to hygiene practices, hard water, and low humidity in winter.
47	Yellow	Describes lesions with lipid, keratin, or bile pigment.	Seen in xanthomas, sebaceous discharge, and bacterial pustules.

A.3 Choice of Anatomical Site

We developed our body region taxonomy by aligning it with how dermatologists reason through diagnoses in clinical settings. Standard references such as *Rook's Dermatology* [9], *Fitzpatrick's Dermatology*, and *Bolognia's Dermatology* [3] consistently describe skin conditions based on their anatomical distribution. These texts emphasize that lesion location plays a central role in diagnosis, distinguishing, for example, mucosal from cutaneous presentations. By mirroring these clinically

grounded patterns, we ensured that our descriptors reflect the spatial logic used in real-world diagnostic workflows.

Coverage gaps in existing datasets: We reviewed widely used dermatology datasets—ISIC, Fitzpatrick17k [10], SD-198 [33], etc., and found that they often lack precise anatomical context. Most provide cropped images that obscure lesion location or annotate broad categories like "face" or "limb," limiting their clinical utility. To address this, we explicitly included underrepresented yet diagnostically critical regions such as the armpits and groin area. These regions are key to diagnosing conditions like candidiasis and tinea infections.

Hierarchical design for diagnostic reasoning: We designed our annotation hierarchy to support models that reason at multiple anatomical resolutions. Dermatologists often start with coarse region-based hypotheses and further refine them until morphology and context become clearer. Our taxonomy enables similar flexibility, allowing models to learn general patterns at macro levels while capturing fine-grained distinctions when needed. This structure mirrors how clinicians disambiguate conditions with overlapping visual features based on location. The complete list of anatomical regions used in our annotation schema is provided in the Datasheet included with the supplementary material for reference.

A.4 Comparative Coverage of Dermatological Disease Categories Across Public Datasets

Most publicly available dermatology datasets were developed for specific diagnostic tasks, often skin cancer triage, and do not reflect the full diagnostic spectrum seen in routine outpatient clinics, particularly in low and middle-income countries (LMICs) where poor maintenance of hygiene amongst the population is a key factor for the spread of infectious diseases. As a result, critical categories such as infectious disorders, pigmentary changes, and appendageal conditions are underrepresented or absent entirely. To assess where our dataset stands in relation to existing benchmarks, we compiled an exhaustive comparison in the Sup. Table 5 of major dermatology datasets across clinically meaningful diagnostic categories.

Table 5: Comparative distribution (in %) of dermatological disease categories across public datasets. Only our dataset provides a good representation across all categories as encountered in routine outpatient care, including mixed diagnoses.

Dataset	Infectious	Inflammatory (incl. keratinisation)	Pigmentary	Appendageal (Acne/Hair)	Neoplastic	No Definite Diagnosis	Others	Key Observations
DermaCon-IN	40.86	30.53	15.25	8.81	0.95	0.68	2.92	Full-spectrum, OPD-aligned dataset designed for LMIC clinical diversity
SCIN [40]	21.85	56.5	0.75	Sparse	5.20	Not included	15.0	Inflammatory-heavy; lacks uncertain and appendageal representation
Fitzpatrick17k [10]	–	65.67	7.2	Sparse	26.7	Not included	–	Inflammatory and neoplastic skew; lacks diagnostic uncertainty
PASSION [8]	63.52	25.05	Sparse	–	–	Not included	11.43	Pediatric LMIC dataset; lacks neoplastic and appendageal coverage
DDI [4]	1.66	2.28	0.46	Sparse	92.7	Not included	3.0	Biopsy-focused dataset; neoplasm-dominant
ISIC 2020 [17]	–	–	–	–	100.00	Not included	–	Exclusive neoplasm dataset
PH2 [26]	–	–	–	–	100.00	Not included	–	Exclusive neoplasm dataset
HAM10k [37]	–	–	–	–	100.00	Not included	–	Exclusive neoplasm dataset
PAD-UFES [28]	–	–	–	–	100.00	Not included	–	Cancer-focused dataset only

A.5 Other stats of the DermaCon-IN dataset

Demographic and Phenotypic Distribution: The dataset reveals distinct demographic and phenotypic trends across age, sex, and skin tone that shape its clinical composition (Sup. Figure 11). Most images are concentrated in the 20–40 age group, with secondary peaks in 10–20 and 40–60, reflecting outpatient demand among working-age individuals. Children (0–10) and older adults (60+) are relatively underrepresented. A notable sex imbalance exists, with males contributing more samples (3394 vs. 2056), possibly due to sociocultural factors. Infectious and pigmentary disorders
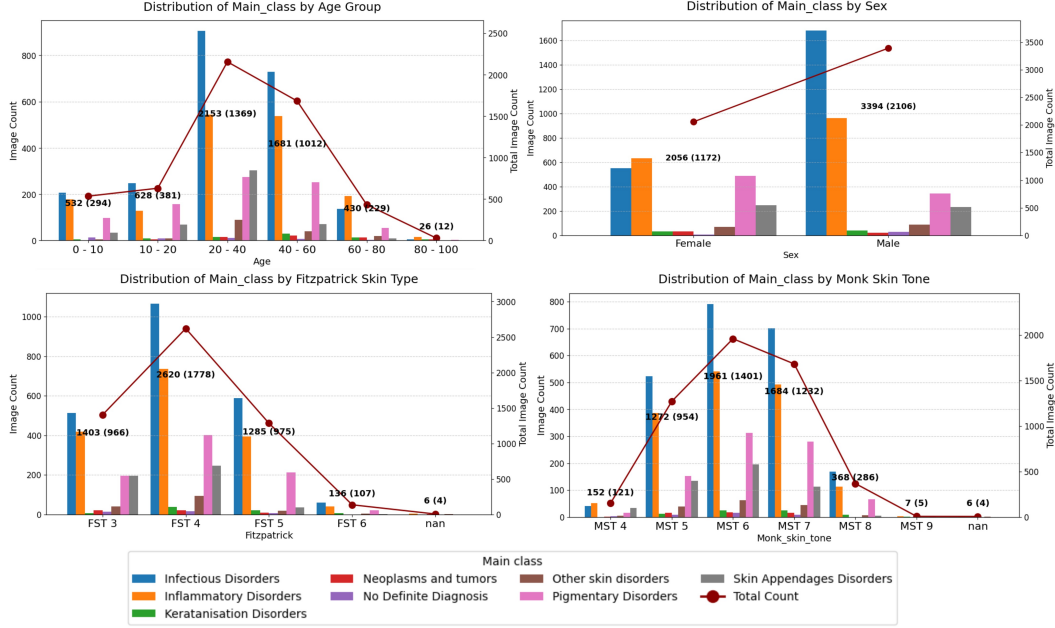
Figure 11: Plots for distribution of dermatological Main Classes (MC) across patient demographics. Each bar represents the number of images per category (Age group, Fitzpatrick type, Monk Skin Tone, or Sex), while the red line denotes the total number of images. Numeric annotations above each point indicate image count followed by subject count in parentheses.

dominate across both sexes, with females also showing higher counts for appendageal and inflammatory conditions.

In terms of skin tone, Fitzpatrick Types 4 and 5 are most prevalent, followed by Type 3. Type 6 is modestly represented (136 images), but is still less frequent relative to mid-tone categories. The Monk Skin Tone distribution similarly centers on MST 6 and 7, with lighter (MST 4) and darker tones (MST 8–9) less represented. Across all groups, infectious, inflammatory, and pigmentary disorders remain most common.

Concept Distribution: A detailed analysis of the concept counts per Main class is presented in Sup. Fig. 12. The figure demonstrates the occurrence of shared concepts across the main class. Further, it also suggests an imbalance of concepts within each class.

B   Model Architecture Details

B.1   Concept Bottleneck Modeling

We investigate two modeling variants under the Concept Bottleneck framework: a 1-level CBM that performs either main class (MC) or sub-class (SC) prediction independently, and a 2-level CBM that jointly predicts both levels in a hierarchical structure. While both designs share a common concept encoder comprising a Swin Transformer followed by dropout and a linear projection to produce concept logits c^l, they differ in their classification strategies as discussed below. Architectural and training hyperparameters for all CBM variants are summarized in Sup. Table 6.

B.1.1   1-level CBM for MC/ SC Classification

To explore the utility of medically grounded concepts in isolation, we train a Concept Bottleneck Model (CBM) that predicts dermatological categories, either main classes (MC) or sub-classes (SC), directly from concept representations. This model maps image features to concept logits and performs classification using those logits alone.

17

Figure 12: Circular plots of counts of Concepts (both skin lesion descriptors and body parts) for each main class skin labels.

Model Architecture. An input image $x \in \mathbb{R}^{3 \times H \times W}$ is first passed through a Swin Transformer backbone to extract a feature embedding. This embedding is then followed by a fully connected projection having Dropout, to produce a concept logit vector:

$$c^l = \texttt{Linear}(\texttt{Dropout}(\texttt{SwinTransformer}(x))) \in \mathbb{R}^K$$

The raw concept logits c^l are used as input to a linear classification head:

$$y = f(c^l)$$

where $f(\cdot)$ is a single-layer classifier mapping to either subclass or main class logits depending on the training objective.

Training Objective. The model is trained with two primary losses:

$$\mathcal{L}_{\text{concept}} = \text{BCEWithLogits}(c^l, c_{\text{true}})$$
$$\mathcal{L}_{\text{class}} = \text{CrossEntropy}(f(c^l), y_{\text{true}})$$

18

The total loss is:

$$\mathcal{L}_{\text{total}} = \mathcal{L}_{\text{concept}} + \mathcal{L}_{\text{class}} + \lambda \|c^l\|_1$$

An L1 regularization term encourages sparsity in the concept representation, invoking the relevant concepts, improving interpretability, and acting as a regularizer during optimization.

Sampling and Imbalance Handling. To account for label imbalance in the main class distribution, we compute per-sample weights based on the inverse frequency of the main class and use a `WeightedRandomSampler` during training.

Table 6: Training and architecture hyperparameters for all CBM models.

Component	Value / Setting
Backbone architecture	Swin-B (patch4, window12, 384)
Image resolution	512×512
Concept vector dimension K	96
Dropout before concept head	0.3
Concept supervision loss	BCEWithLogits (sigmoid applied internally)
Task heads $f(\cdot), g(\cdot)$	Linear layers (no hidden layer)
SC/MC loss	CrossEntropy with label smoothing $\epsilon = 0.1$
L1 regularization weight λ	1×10^{-4}
Optimizer	AdamW
Learning rate	3×10^{-5}
Weight decay	1×10^{-4}
Scheduler	CosineAnnealingLR (T_{max}=30, min LR=10^{-6})
Training epochs	40
Batch size	130 (2-level), 100 (1-level)
Multi-GPU support	DataParallel (4 GPUs)

B.1.2 2-level CBM for MC & SC Classification

We propose a two-level hierarchical prediction framework based on Concept Bottleneck Models (CBMs), where disease predictions are structured via an interpretable intermediate layer of clinical concepts (refer Fig. 7 of the main paper). The task is to jointly predict a fine-grained dermatological *sub-class* label $y^1 \in \{1, \ldots, N_{\text{sub}}\}$ and a coarser *main class* label $y^2 \in \{1, \ldots, N_{\text{main}}\}$, from an input image $x \in \mathbb{R}^{3 \times H \times W}$.

Concept Space. A vision backbone (Swin Transformer) maps the input image to a K-dimensional concept logit vector:

$$c^l = \texttt{Linear}(\texttt{Dropout}(\texttt{SwinTransformer}(x))) \in \mathbb{R}^K$$

We define $c = \sigma(c^l) \in [0,1]^K$ as the sigmoid-activated concept probabilities, which are supervised using binary multi-label concept annotations. The raw logits c^l, not the sigmoid outputs, are further used for downstream disease classification, preserving gradient flow and avoiding saturation effects.

Type 1: Cascade Architecture. This model enforces taxonomy consistency by chaining predictions through intermediate subclass logits:

$$y^1 = f(c^l), \quad y^2 = g(y^1)$$

Here, $f(\cdot)$ is a linear layer mapping concept logits to subclass logits $\in \mathbb{R}^{N_{\text{sub}}}$, and $g(\cdot)$ is another linear layer mapping subclass logits to main class logits $\in \mathbb{R}^{N_{\text{main}}}$. This design structurally enforces taxonomic consistency between sub- and main classes, aligning with medical hierarchies. However, performance is inherently constrained by the reliability of the first-stage prediction y^1, making it prone to error propagation.

Type 2: Parallel Architecture. Instead of sequential dependency, both SC and MC are predicted directly from concept logits:

$$y^1 = f(c^l), \quad y^2 = g(c^l)$$

Here, $f(\cdot)$ and $g(\cdot)$ are task-specific linear classifiers. This decouples the learning paths while maintaining shared semantic grounding via concepts. The architecture benefits from multi-task

supervision and avoids dependency on intermediate task outputs. It allows the model to flexibly learn patterns that are specific to either task while still being grounded in a common, interpretable representation.

Loss Function.   The overall objective for each image includes:

- Binary cross-entropy loss on sigmoid-transformed concepts:

$$\mathcal{L}_{\text{concept}} = \text{BCEWithLogits}(c^l, c_{\text{true}})$$

- Cross-entropy loss on subclass logits:

$$\mathcal{L}_{\text{SC}} = \text{CrossEntropy}(f(c^l), y^1_{\text{true}})$$

- Cross-entropy loss on main class logits:

$$\mathcal{L}_{\text{MC}} = \begin{cases} \text{CrossEntropy}(g(y^1), y^2_{\text{true}}), & \text{Type 1} \\ \text{CrossEntropy}(g(c^l), y^2_{\text{true}}), & \text{Type 2} \end{cases}$$

- L1 regularization on concept logits to promote sparsity:

$$\mathcal{L}_{\text{L1}} = \lambda \|c^l\|_1$$

The total loss is:

$$\mathcal{L}_{\text{total}} = \mathcal{L}_{\text{concept}} + \mathcal{L}_{\text{SC}} + \mathcal{L}_{\text{MC}} + \mathcal{L}_{\text{L1}}$$

Class Imbalance Handling.   To account for imbalanced subclass and main class distributions, we assign sample-wise weights based on inverse frequency. For each sample i, the final weight is computed as:

$$w_i = \frac{1}{2}\left(\frac{1}{f(y^1_i)} + \frac{1}{f(y^2_i)}\right)$$

where $f(\cdot)$ is the empirical class frequency. These weights are used with a `WeightedRandomSampler` to ensure that rare classes contribute adequately during training.

B.1.3   Handling Variable Image Resolutions.

Dermatological images in real-world clinical datasets often exhibit heterogeneous resolutions and aspect ratios. To address this, we first resize images such that their longer side does not exceed 512 pixels while maintaining the aspect ratio. The resized image is then zero-padded to 512×512 to ensure uniform input dimensions across batches. This approach preserves image content without distortion and enables efficient batch processing while maintaining compatibility with the fixed input size expected by the Swin Transformer backbone. Padding is handled dynamically during training and validation through a custom collate function.

B.2   Detailed Performance Analysis

Main Class Classification Performance.   Sup. Table 7 presents a detailed evaluation of our best-performing models for main class (MC) prediction. We report Top-1, Top-3, and Top-5 classification accuracies along with macro AUC values (%) across all main classes and per-class breakdowns.

For example, in inflammatory and pigmentary disorders, Top-1 accuracies range between 65–73%, but Top-5 scores consistently rise above 95%, indicating that the correct class is almost always among the top few ranked predictions. This pattern holds across infectious and appendageal disorders as well, with Top-5 accuracy approaching ceiling levels (above 97% in most cases). Such trends affirm the model's capacity to capture relevant features even in challenging differential diagnosis.

Conversely, classes such as Keratinisation disorders, Neoplasms, others and no diagnosis exhibit lower Top-1 performance, yet still benefit from 20–40% absolute improvement when considering Top-5 predictions. This suggests that while these categories are harder to pinpoint as the top choice, the model often recognizes them as plausible alternatives, supporting their inclusion in a ranked differential. This reflects the inherent difficulty or class imbalance in these categories. These results highlight strong discriminative performance in clinically prevalent and visually distinct categories, while also pointing to the need for improvement in more ambiguous or underrepresented classes.

Table 7: Detailed performance analysis of best models for main class (MC) prediction. All metrics include Accuracy (Top-1,3,5) and AUC (ovr) as % for both: all classes and per class.

Model	Metric	All classes	Infectious	Inflammatory	Keratanisation	Neoplasms	No Diagnosis	Other	Pigmentary	Appendages
Swin (MC)	Top-1	70.88	77.51	68.51	14.29	16.67	0.00	14.29	73.17	81.19
	Top-3	91.06	94.98	96.10	50.00	83.33	33.33	32.14	87.20	92.08
	Top-5	94.86	97.13	98.70	50.00	83.33	66.67	60.71	92.07	97.03
	AUC	78.36	84.80	82.76	66.29	87.05	55.55	63.57	91.11	95.79
CBM (Concepts+ MC)	Top-1	67.55	72.49	67.21	7.14	25.00	0.00	7.14	70.73	77.23
	Top-3	91.72	98.33	96.75	21.43	41.67	16.67	32.14	89.02	90.10
	Top-5	96.57	99.52	99.68	57.14	83.33	66.67	60.71	94.51	97.03
	AUC	79.17	85.70	81.80	56.40	79.10	74.34	68.60	93.09	94.37
CBM Type 2 (Concepts+ MC & SC)	Top-1	70.12	79.43	66.23	7.14	16.67	0.00	14.29	71.95	75.25
	Top-3	90.49	94.50	96.43	14.29	41.67	33.33	46.43	87.80	92.08
	Top-5	95.53	95.93	99.03	64.29	75.00	66.67	82.14	95.73	95.05
	AUC	78.71	84.78	83.08	66.30	80.62	60.91	68.39	91.77	93.82

C   More examples for Post-hoc analysis

The following post-hoc analyses are conducted using the best-performing CBM, namely the Type-2 model, on the test set provided in GitHub.

C.1   Concept Activation Analysis

We analyzed the activation patterns of interpretable concepts across eight dermatological disorder categories to evaluate semantic alignment in model reasoning. Concepts were grouped into two clinically motivated families: *descriptor* concepts (e.g., *plaque*, *erythema*, *vesicle*) and *body part*
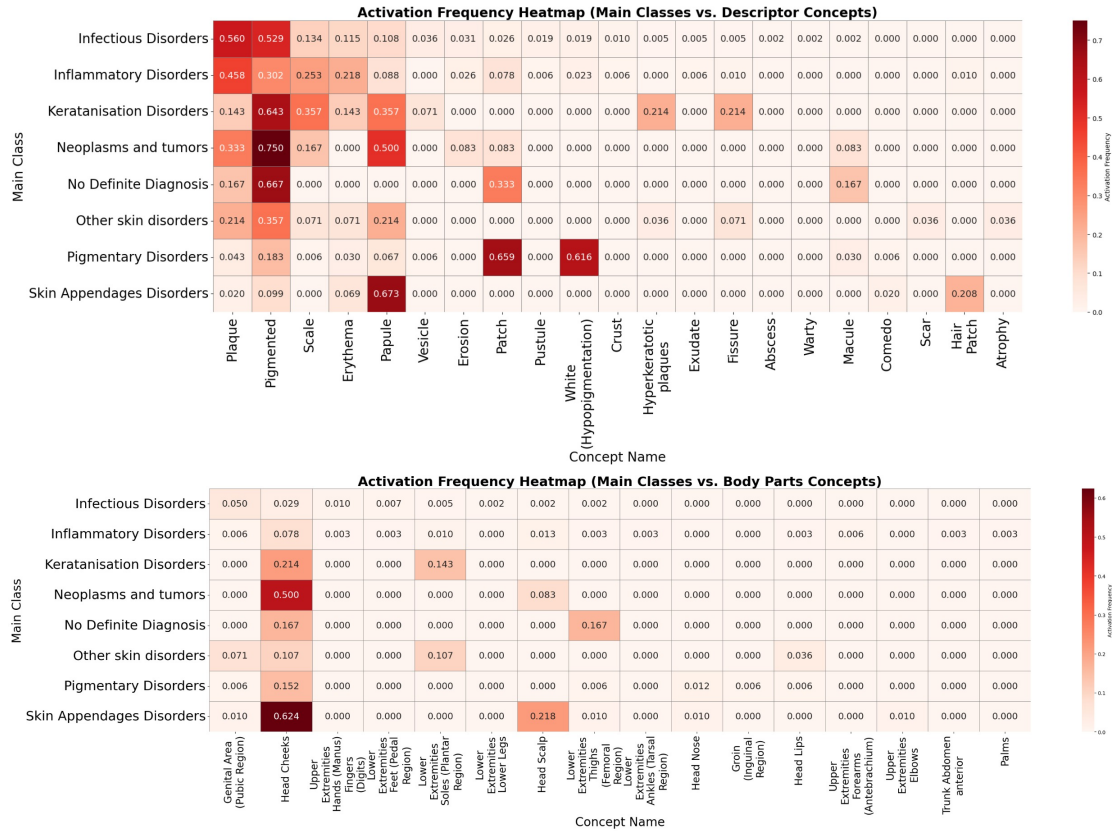

Figure 13: Concept frequency heatmaps for the analysis of active concepts per class (Main class) on the full test set.

concepts (e.g., *head*, *cheek*, *extremities*). For each class, activation frequency was computed as the fraction of samples per class in which a given concept was predicted to be positively active and is presented as heatmaps in Sup. Fig. 13. Concepts with negative activation across all classes were excluded from visualization.

Out of 47 available descriptor concepts, 21 exhibited positive activation. For body part concepts, 16 out of 49 exhibited positive activation. This indicates that the model's decision process selectively emphasizes a small subset of clinically relevant features while disregarding many others, which could be due to lower predictive value.

Notably, descriptor activations showed meaningful alignment with known disease characteristics: *papule* and *pigmented* were strongly associated with *Skin Appendages Disorders* and *Neoplasms and Tumors* respectively, while *Pigmentary Disorders* prominently activated *patch* and *white hypopigmentation*. In contrast, body part activations were more sparse and concentrated, with only a few regions such as *head cheeks*, *head scalp*, and *lower extremities thighs* contributing meaningfully. The under-utilization of many anatomical concepts possibly suggests the model's insensitivity to spatial context.

This selective concept usage underscores the need for additional constraints that promote semantic coverage and balanced concept learning. Future work could incorporate concept entropy regularization or supervision-aware attention mechanisms to encourage more uniform engagement across the concept space, particularly for underrepresented anatomical regions.

C.2 Concept Contribution Analysis Across Semantically Disjoint Families

To further explore the interplay between *descriptor* and *anatomical* concept families within our Concept Bottleneck Model (CBM), we provide two sets of illustrative examples (Sup. Fig. 14, 15). These were chosen from correctly predicted samples with concept annotations verified by expert dermatologists. Contribution scores are computed using signed, log-scaled intermediate logits, reflecting each concept's influence (positive or negative) on the final class prediction.

(a) Positive Contribution from Body Part Concepts with Co-activation of Descriptors. In Sup. Fig. 14, we show eight representative cases where at least one body part concept has a positive contribution to the model's decision. In seven of these, we observe concurrent positive contributions from descriptor concepts, as well, suggesting that when anatomical information is utilized by the model, it is rarely used in isolation. Only one sample showed no positively contributing descriptor, which may hint at either spurious localization or weak feature learning from descriptors in that particular case. This consistent pattern of joint activation supports the view that meaningful spatial reasoning in the model emerges most reliably when supported by surface-level lesion features, reinforcing the clinical validity of concept co-activation as a desirable property in interpretable models.

(b) Dominance of Descriptor Concepts in Prediction with Absent Positive Anatomical Contributions. Sup. Fig. 15 complements the above by presenting eight cases where descriptor concepts show strong positive contributions, but none of the body part concepts make a positive impact. While both positively and negatively contributing concepts are visible, the absence of anatomical contributions even in correctly classified examples highlights the model's stronger reliance on surface-level lesion descriptors.

These observations are consistent with the concept frequency analysis reported earlier, where descriptor concepts not only activated more frequently but also aligned more closely with disease-specific patterns. Taken together, these findings reveal a clear representational bias in the CBM toward the descriptor concept family, underscoring the need for regularization strategies or balanced supervision to ensure equitable utilization of spatial and morphological information.

C.3 Concept-specific Spatial Attribution via Grad-CAM

To gain spatial interpretability over concept activations, we performed Grad-CAM analysis on the Swin Transformer's CBM layer for a subset of correctly classified examples. As illustrated in Sup. Fig. 16, each visualization corresponds to a specific concept with positive contribution selected from the CBM's intermediate bottleneck (e.g., *plaque*, *scale*, *palms*), with ten examples chosen to demonstrate the range and specificity of concept-localized attention. Using logit-directed gradient

Figure 14: Bar plots showing the top and bottom-k contributing concepts (lesion descriptors and body parts) for the model's prediction. Contribution values are computed as signed, log-scaled scores derived from the CBM's intermediate concept logits. Blue bars indicate the concepts with positive contributions, whereas the red bars highlight the concepts with negative contributions, and all are rightly predicted. These examples specifically highlight cases where at least one body part concept has a positive contribution, with lesion descriptors also showing concurrent scores in most instances.

Image with Prediction	Lesion Descriptor Concepts with scores	Body Parts Concepts with scores

Infectious Disorders

Plaque +1.1
Pigmented +0.3
Scale +0.1
Excoriation -2.4
Exophytic/Fungating -2.5

Perianal Area -2.4
Trunk Abdomen Navel -2.4
Head Lips -2.5

Infectious Disorders

Plaque +0.6
Erosion +0.5
Erythema +0.4
Exudate +0.4
Crust +0.3
Lichenification -2.6
Wheal -2.6

Head Lips -2.4
Nails Fingernails -2.5
Lower Extremities Thighs -2.5

Infectious Disorders

Scale +0.8
Plaque +0.7
Erosion +0.5
Pigmented +0.3
Yellow -2.5
Lichenification -2.7

Head Eye -2.4
Head Lips -2.5
Nails Fingernails -2.7

Neoplasms and tumors

Erosion +0.4
Erythema +0.2
Plaque +0.1
Wheal -2.3
Flat-topped -2.5

Lower Extremities Lower Legs -2.4
Calves -2.4
Navel -2.5

Inflammatory Disorders

Scale +1.0
Plaque +0.9
Erythema +0.9
Dilated Vein -2.6
Warty -2.7

Groin -2.4
LowerBack -2.4
Nails Toenails -2.7

Inflammatory Disorders

Plaque +0.8
Pigmented +0.4
Scale +0.4
Telangiectasia -2.7
Hair Patch -2.7

Mucous Membranes Oral Cavity -2.5
Armpits -2.6
Nails Toenails -2.7

Infectious Disorders

Plaque +1.0
Pigmented +0.0
Xerosis -2.4
Excoriation -2.5
Exophytic/Fungating -2.6

Head Eye -2.4
Perianal Area -2.4
Head Lips -2.5

Other skin disorders

Scar +0.8
Pigmented +0.7
Atrophy +0.4
Warty -2.5
Burrow -2.6

LowerBack -2.5
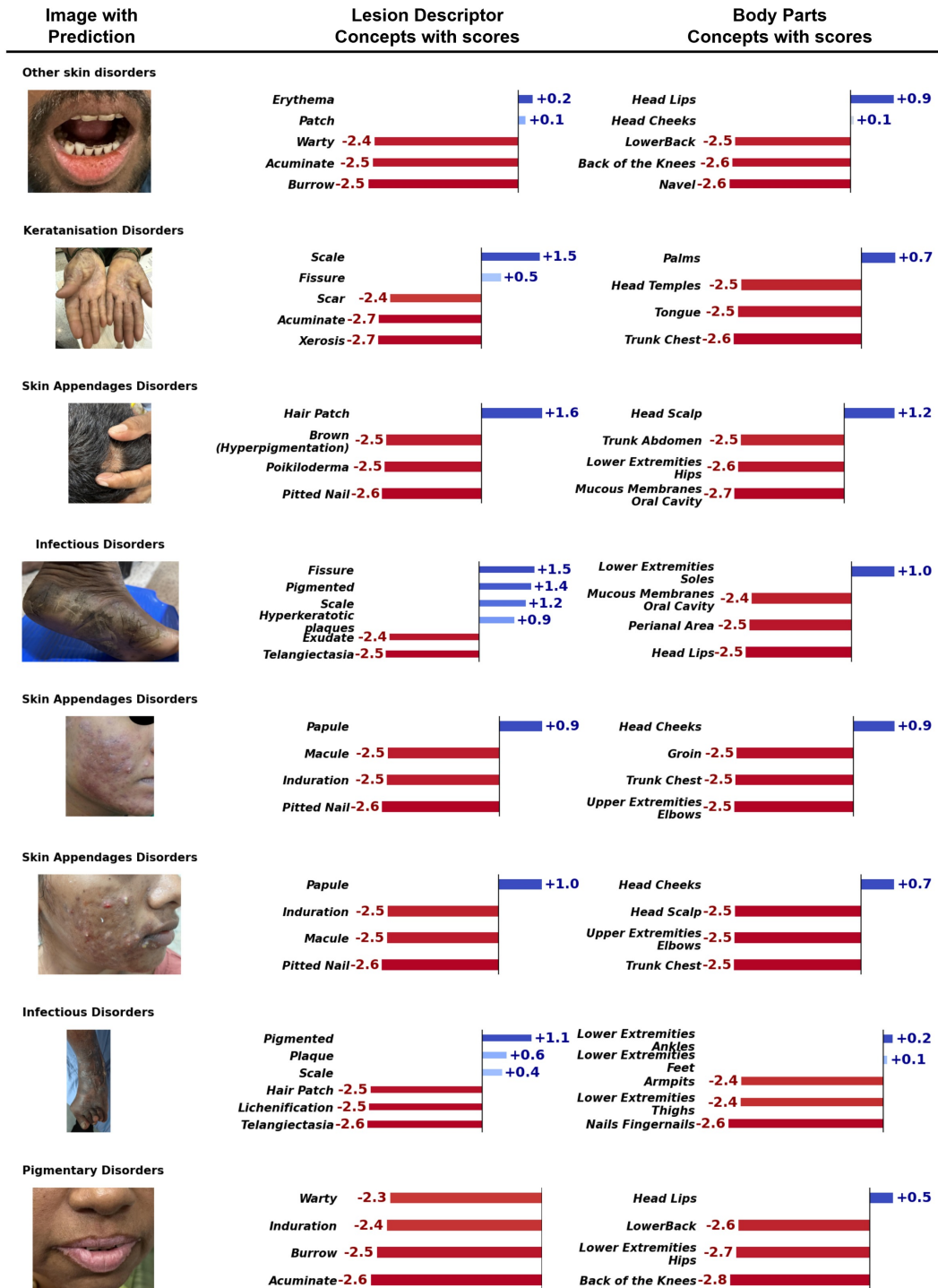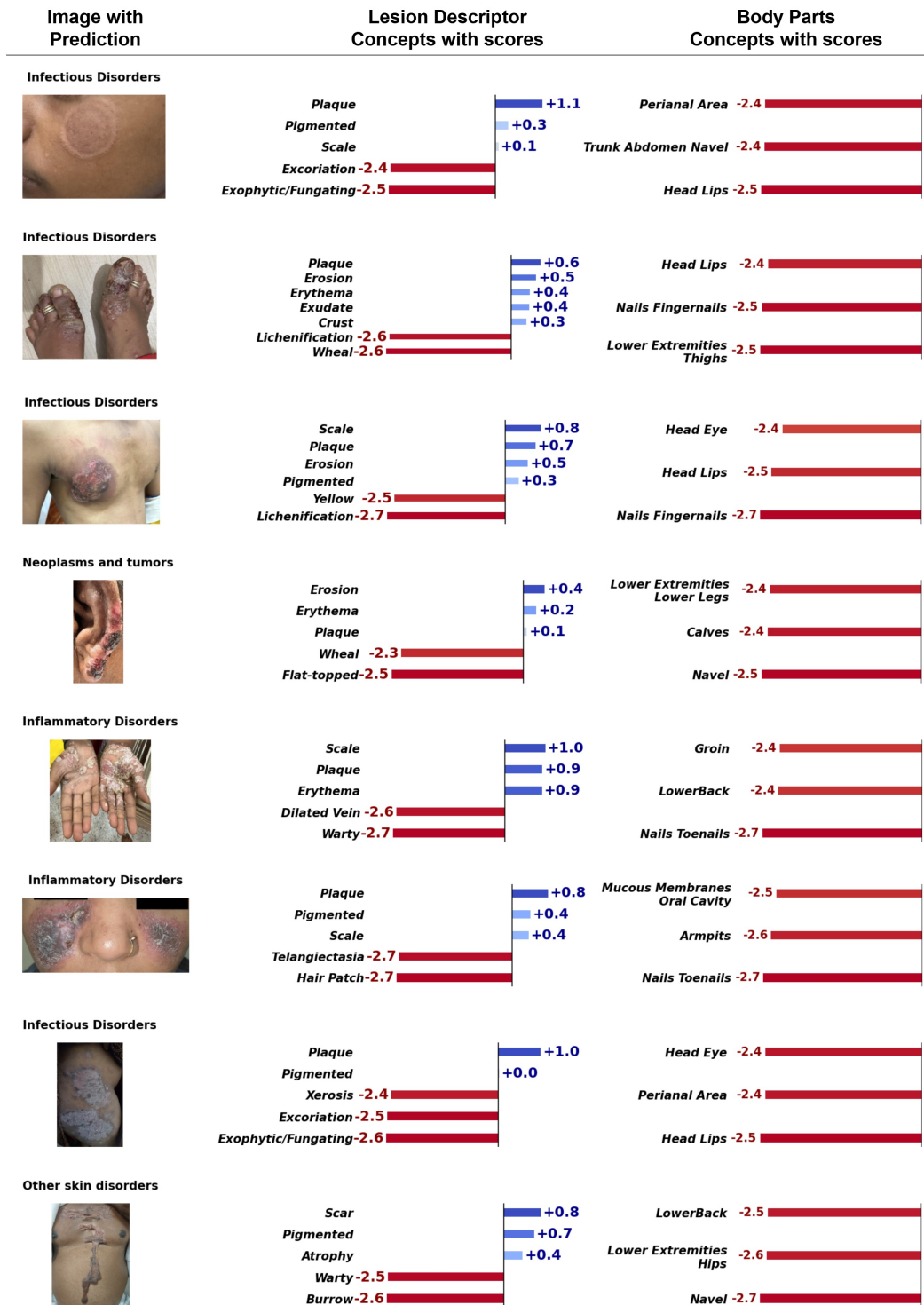Lower Extremities Hips -2.6
Navel -2.7

Figure 15: Bar plots showing the top and bottom-k contributing concepts (lesion descriptors and body parts) for the model's prediction. Contribution values are computed as signed, log-scaled scores derived from the CBM's intermediate concept logits. Blue bars indicate the concepts with positive contributions, whereas the red bars highlight the concepts with negative contributions, and all are rightly predicted. These examples specifically highlight cases where at least one lesion descriptor concept has a positive contribution, while body part concepts exhibit negative contribution.
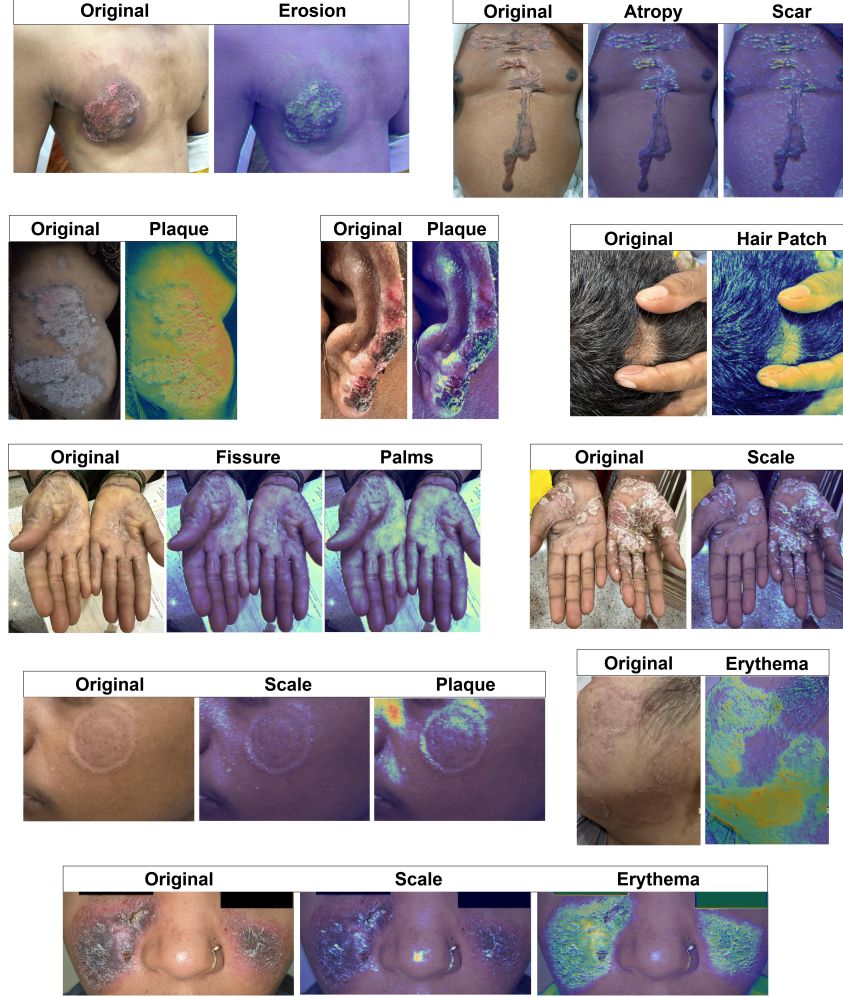
Figure 16: Illustrations of Grad-cam visualizations over Swin Transformer by choosing a specific concept. Highlighted parts of the images with either green, yellow, or red points to the regions responsible for the positive contribution of the concept. All the images were further cross-validated by the dermatologists for the right concept activation.

backpropagation from the concept prediction head, we generated class-discriminative heatmaps that reveal the spatial regions influencing each concept's activation. These visualizations reinforce the semantic alignment between model representations and clinical reasoning: lesion descriptors such as *erythema* or *plaque* consistently activate in regions of visible inflammation or raised morphology. Importantly, the ability to isolate spatial attributions per concept allows clinicians to verify not just *what* the model has learned, but also *where* it is looking, serving as a crucial step toward validating model trustworthiness in clinical settings.

D   Cross-Dataset Validation and Distributional Coverage

Our dataset has been developed with a focus on flexibility and interoperability, aiming to support a range of downstream dermatological AI tasks. Its hierarchical taxonomy enables researchers to adjust label granularity according to their specific objectives, whether for disease classification, concept prediction, or region-aware modeling.

To demonstrate this integrative potential, we conducted cross-dataset evaluations using two publicly available benchmarks: the PASSION [8] dataset and the Fitzpatrick17k [10] dataset. Using our label hierarchy, we aligned 40 randomly selected samples (due to unavailability of val splits) from each dataset to our taxonomy, as the label space for both datasets was different. The best performing CBM
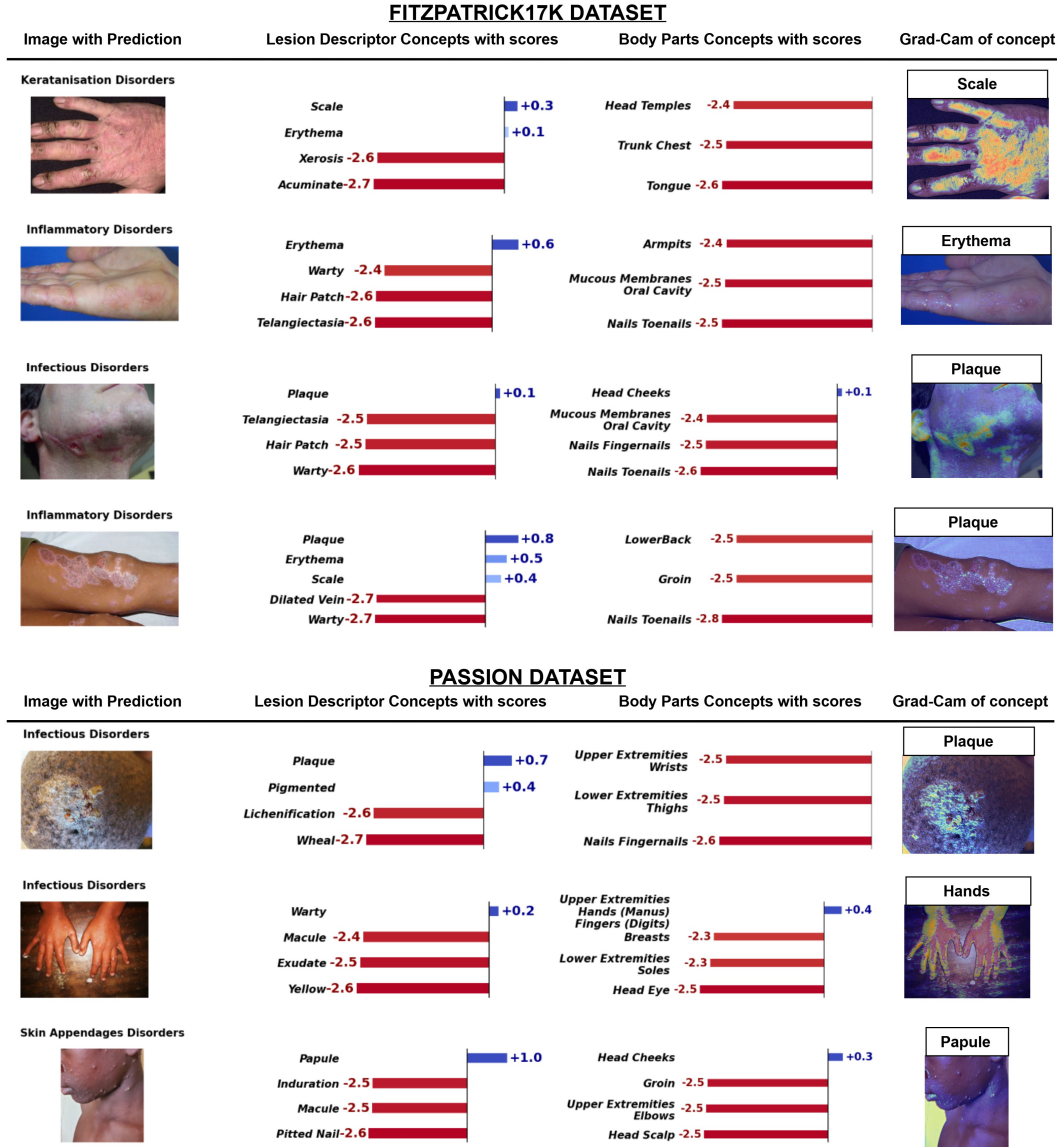
Figure 17: Illustration of interpretability analysis of CBM (Type 2) model trained on DermaCon-IN dataset and cross validated on samples of Fitzpatrick17k and PASSION datasets. Bar plots show the top and bottom-k contributing concepts (lesion descriptors and body parts) for the model's prediction. Contribution values are computed as signed, log-scaled scores derived from the CBM's intermediate concept logits. Blue bars indicate the concepts with positive contributions, whereas the red bars highlight the concepts with negative contributions, and all are rightly predicted. The rightmost column presents the Grad-Cam analysis of the best concept.

(Type 2) model, trained exclusively on DermaCon-IN dataset, correctly predicted 30 samples from PASSION and 33 from Fitzpatrick17k, and produced clinically valid and interpretable Grad-CAM visualizations across these external samples. All outputs were reviewed and verified by a board-certified dermatologist for both diagnostic accuracy and localisation relevance. A few samples of our analysis is presented in Sup. Fig. 17.

These observations suggest that our dataset is neither isolated nor out-of-distribution. Rather, it addresses a critical representational gap by contributing cases from underrepresented skin tones, outpatient clinical settings, and real-world diagnostic variation specific to South Asian populations.

While further large-scale benchmarking is necessary, our results suggest that the structure and diversity of the dataset provide practical value for researchers dealing with heterogeneous dermatological data. Although we do not claim generalisability, the dataset can be an asset for training models aimed towards transferability and foundational learning.

E   Ethical Considerations

This dataset was curated through clinical data collection from consenting patients from outpatient clinics. Ethical diligence was integrated into the dataset lifecycle, including data collection, annotation, privacy protection, and intended use, in line with emerging best practices for responsible dataset curation in human-centric computer vision (HCCV). The protocol was reviewed and approved by the institutional ethics committee.

Data Source and Informed Consent   All images were collected during routine dermatological consultations with informed consent from patients in the native language or a language more easily understood by the patients. No data was scraped from the web or obtained from public platforms.

Privacy Protection and Anonymization   We ensured that no personally identifiable information (PII) was present in any image and is irreversibly coded for identity. Facial identifiable features such as eyes, tattoos, and other identifiable marks were excluded or cropped from the images. Additionally, all embedded metadata (e.g., timestamps, device IDs, location data) was removed. Participants were informed of their right to withdraw from the study.

Cultural Sensitivity.   During image collection involving female patients, all study procedures were explained by, or in the presence of, female medical staff to ensure comfort, privacy, and culturally appropriate engagement.

Annotation Integrity and Labeling Ethics   All annotations were carried out by trained clinical annotators working under dermatologist supervision. We deliberately avoided inferring any identity-related attributes from images. Skin tone annotations were made directly based on non-affected skin regions using standardized MST/Fitzpatrick reference scales. Inter-annotator consistency was maintained through calibration sessions, and difficult cases were adjudicated by a senior dermatologist.

Use Restrictions and Responsible Deployment   The dataset is intended for academic research, particularly in studying fairness, robustness, and interpretability in dermatological disease classification. It is not intended for commercial use, biometric profiling, identity inference, or deployment in real-time diagnostic tools without regulatory and clinical validation. We intend to make the dataset openly accessible to support research in dermatological AI. However, access will be granted following a background verification process to ensure responsible and ethical use.

F   Societal Impact

The potential impact of this dataset lies not in the scale of data amassed, but in its grounding within everyday clinical reality. By capturing routine skin conditions in South Asian outpatient settings, where diagnostic decisions often occur with limited advanced imaging, the dataset reflects how dermatological care is actually practiced in many parts of the world. Its value, therefore, is not just in building algorithms, but in offering a testbed where machine learning systems can be evaluated under conditions that mirror frontline clinical environments. Additionally, by organizing information

through interpretable clinical descriptors and anatomical context, the dataset invites collaboration between clinicians and model developers, not as a retrospective audit, but as an integral part of design. This is particularly meaningful for low-resource settings where human expertise must be complemented. Rather than aiming for universal solutions, we hope this dataset contributes to a shift toward more situated, dialogic approaches to clinical AI development.

Beyond its immediate utility for algorithm training, the dataset also raises possibilities for advancing how uncertainty and variability are treated in clinical AI. By including lesions with atypical or overlapping features, cases that might otherwise be excluded, it encourages models to engage with diagnostic edge cases rather than avoid them. This is particularly relevant in primary care and peripheral settings, where clear-cut presentations are the exception, not the norm. Additionally, the dataset provides opportunities to study how different combinations of features influence clinical suspicion, enabling future work on model calibration and risk stratification. In this way, the dataset serves not only as input to predictive systems and as a scaffold for developing tools that assist with triage, escalation decisions, or patient education — areas where uncertainty is not a flaw but a central part of the task.

G   Glossary of Terms

Table 8: Glossary continued across pages.

Term	Definition
Alterations	Alterations denote clinically observable changes in lesion attributes such as color, texture, or size over time, often indicating progression, regression, or therapeutic response.
Anatomical	Anatomical refers to the specific bodily region where a lesion appears, which can influence diagnostic reasoning due to region-specific disease prevalence and morphology.
Anomalies	Anomalies represent structural or morphological deviations from typical presentation, often indicating pathological states like vascular malformations or congenital disabilities.
Appendageal	Appendageal pertains to skin-associated structures such as hair follicles, sebaceous glands, and nails, diagnostically relevant in conditions like alopecia or onychomycosis.
Atopic	Atopic describes conditions driven by hypersensitivity or allergic predisposition, notably atopic dermatitis, often linked to genetic and environmental triggers.
Blistering	Blistering refers to fluid-filled skin elevations (vesicles/bullae).
Chronic	Chronic refers to a Long-standing or recurrent condition; affects annotation and model expectations.
Corticosteroid	Corticosteroid refers to the Anti-inflammatory drug class; often implicated in misuse or treatment.
Curricula	Curricula refers to Formal educational content; provides background for how clinicians interpret and label data.
Cutaneous	Relating to the skin; distinguishes from mucosal involvement.
Demographic	Relating to population traits; crucial for fairness and representation.
Dermatological	About the skin and its diseases; defines the scope of the dataset.
Dermatophytosis	Dermatophytosis refers to a Fungal infection of skin, hair, or nails.
Dermatoses	Dermatoses refers to a general term for skin diseases.
Dermis	Dermis refers to the middle layer of skin, site of many dermatological processes.
Dermoscopy	Dermoscopy is a non-invasive skin imaging technique for assessing pigmented lesions.
Diagnostic	Related to identifying diseases; informs how images are labeled.
Endemic	Regularly found among a population; informs dataset collection region.
Epidemiologically	In terms of disease patterns in populations; informs dataset design.
Epidermis	Epidermis refers to the outer skin layer, involved in superficial lesions and visual markers.
Erosion	Erosion refers to the loss of part of the epidermis; visible and diagnosable via image.
Etiology	The cause or origin of a disease; critical for understanding disease mechanisms in datasets.
Exogenous	Exogenous refers to originating outside the body; affects classification of environmental skin damage.
Fluctuant	Fluctuant refers to Soft and compressible; indicates the presence of fluid (e.g., cysts, abscesses).
Granulomatous	Related to granuloma formation; chronic inflammation marker.
Hematological	Related to blood or blood-forming organs; systemic diseases may manifest cutaneously.
ICD	ICD refers to the International Classification of Diseases; a standardized coding system used globally for diagnosis and reporting.
Incontinence	In dermatology, refers to pigment incontinence where melanin leaks into the dermis.
Infectious	Caused by pathogens; represents a major disease category in dermatology.
Inflammatory	Involving immune response; another common skin disease category.
Keratinization	Keratinization refers to skin thickening; central in conditions like psoriasis.
LMIC	LMIC refers to Low- and Middle-Income Countries; refers to geographic and economic contexts.
Lesion	Lesion refers to any abnormal area on the skin; the primary subject of dermatological datasets.
Melanin	Melanin refers to Pigment responsible for skin color; key in diagnosing pigmentation disorders.
Melanoma	Melanoma refers to a malignant tumor of melanocytes, a key example of a neoplastic skin lesion.
Morbidity	Morbidity refers to the rate of disease in a population; it helps contextualize dataset relevance.
Morphological	Morphological refers to Concerned with form and structure; describes visual features of lesions.
Mucosal	Mucosal refers to moist linings (e.g., inside mouth); important in systemic diseases.
Neoplastic	Neoplastic refers to abnormal cell growth; includes benign and malignant tumors.
Ontologies	Ontologies refer to Structured vocabularies linking concepts; useful for clinical data labeling.
Outpatient	Outpatient refers to a Healthcare setting where patients are not admitted overnight; a common source of dermatology images.

Term	Definition
Palpable	Able to be felt; clinical term for raised or solid lesions.
Pathological	Related to disease processes; central to diagnosis and data labeling.
Pathophysiology	Pathophysiology refers to functional changes associated with disease; links imaging to mechanisms.
Phenotypic	Phenotypic refers to observable traits or characteristics; crucial for image-based annotations.
Pigment	Pigment refers to coloring matter in skin; changes indicate various disorders such as vitiligo or melasma.
Pigmentary	Pigmentary refers to relating to skin color changes; includes hyper- and hypo-pigmentation.
Pigmentary Alterations	Pigmentary Alterations refers to Changes in skin color, important for diagnosing pigmentation disorders.
Polymorphic	Polymorphic refers to having varied forms; describes diverse visual patterns of lesions.
Primary Lesions	Primary Lesions refers to Initial skin changes (e.g., macule, papule); basis for clinical diagnosis.
Pruritic	Pruritic refers to Itchy; common symptom that guides diagnosis.
Rook's	Rook's refers to Rook's Textbook of Dermatology; a key reference in dermatological classification and clinical teaching.
Secondary Changes	Secondary Changes refer to lesion alterations due to disease progression or external factors.
Subcutaneous	Subcutaneous refers to the layer beneath the dermis composed of fat and connective tissue; affected in deep infections or nodules.
Systemic	Systemic refers to affecting the entire body; differentiates skin manifestations of internal diseases.
Taxonomies	Taxonomies refer to systematic classification of concepts or conditions; essential for dataset organization and ontology mapping.
Varicosities	Varicosities refers to dilated veins; visible skin features relevant in elderly or vascular conditions.
Vascular	Vascular refers to relating to blood vessels; includes lesions like purpura and telangiectasia.
Vasculitis	Vasculitis refers to the Inflammation of blood vessels; can present with palpable purpura.
Vesiculobullous	Vesiculobullous refers to Diseases characterized by vesicles and bullae (e.g., pemphigus).
Xanthomas	Xanthomas refers to Lipid-rich lesions; indicative of metabolic disorders.
Xerotic	Xerotic refers to Dry skin; common in aging and environmental dermatitis.